https://doi.org/10.5194/egusphere-2026-2778
Preprint. Discussion started: 1 June 2026

Focusing of Swell at the Nazaré Submarine Canyon

Gaute Hope[1], Edwin J. Rainville[2], Torunn Irene Seldal[1], Matheus Vieira[3,5], Filippo Bergamasco[4,7], Øyvind Breivik[1,6], Pedro Almeida[3], Alvise Benetazzo[4], Trygve Halsne[1], Cintia Bonanad[3], and Birgitte R. Furevik[1,6]

[1]Norwegian Meteorological Institute, Bergen, Norway.
[2]Applied Physics Lab, University of Washington, Seattle, USA.
[3]+ATLANTIC, Lisbon, Portugal.
[4]Consiglio Nazionale delle Ricerche, Istituto di Scienze Marine, Venice, Italy.
[5]Centre for Marine Technology and Ocean Engineering (CENTEC), University of Lisbon, Instituto Superior Técnico, Lisbon, Portugal.
[6]University of Bergen, Bergen, Norway.
[7]Department of Environmental Sciences, Informatics and Statistics - Ca' Foscari University of Venice, Italy.

Correspondence: Gaute Hope (gauteh@met.no)

Abstract. Steep underwater canyons near the coast can significantly modulate the propagation of long waves. Many canyons share similar dimensions of approximately 150 meters deep thalweg at their terminus, and a sloping continental shelf of about 20 meters within hundred meters of the shoreline. Swell traveling above the shelf is refracted and reflected at the canyon edge, where the phase speed increases abruptly due to the increased depth, resulting in a significantly focused wave field. Outside Nazaré, Portugal, one of the largest near-shore canyons exist, extending to within ten meters of the shoreline. Here, some of the largest breaking waves (> 20 meters) in the world are formed. We deployed arrays of wave buoys above the canyon, and stereo cameras mounted at the cliff at Nazaré overlooking the canyon edge, allowing us to measure the wave field at far greater spatial and temporal resolution than any previous experiment. The swell propagation is modeled using ray tracing and a boundary element method. In particular, the shape of a submarine canyon's edge in the final hundreds of meters toward the coastline is crucial for how and exactly where beams are focused towards the beach. Contrary to the popular explanation that the large waves are channeled through the canyon, we find they are refracted and reflected along the canyon edge. We find that waves longer than about 7 seconds are mostly reflected at the canyon, common to many canyons around the world. At Nazaré, optimal focusing occurs for waves arriving from about $275° — 315°$. This is in agreement with the experience from the surfing community which considers waves arriving from about $290° — 315°$ to yield the biggest surf.

1 Introduction

In the winter, waves exceeding 20 meters, sometimes exceeding 30 meters, are observed before breaking in the surf zone of the northern beach of Nazaré in Portugal. Measurements recorded offshore by wave buoys over the past 15 years point to a maximum wave height of 19.4 meters in deep waters, and recently, waves reaching 20 meters have been accurately measured close to the shore as well. The large waves at Nazaré are a product of North-North-Westerly long-period swell generated in the North Atlantic and the effects of a steep underwater canyon.

https://doi.org/10.5194/egusphere-2026-2778
Preprint. Discussion started: 1 June 2026

Here, we measure for the first time the phase-resolved wave-field across the canyon edge using dense and high-frequency buoy measurements as well as 3D reconstructions of the sea-surface, at far greater spatial and temporal resolution than previous experiments. The refraction of the ocean swell, and the cut-off frequencies for short-waves, are measured and modeled to understand how the geometry of the seafloor cause the wave field to be refracted, reflected and ultimately focused towards the beach.

The northern edge of the canyon, which aligns with the promontory (with the lighthouse) acts to reflect and refract incoming waves towards the Praia do Norte (Northern beach, see Fig. 2a), interfering with the incident wave field. The interference patterns caused by submarine canyons can substantially increasing the amplitude (Lacombe, 1950). Ultimately, the waves shoal and break as they approach the shore. However, multi-directional wave fields, such as those set up at Nazaré, can sustain significantly steeper waves compared to those produced by unidirectional wave systems before they break (McAllister et al., 2024). Large wave events (H_s approaching 10 m) outside the coast of Portugal are shown by wave buoys (Fig. 1) to be yearly events. The result is the formation of several distinct breaking points (commonly referred to as *peaks* within the surf community) where waves rise abruptly out of the water, taking on the shape of towering pyramids (Fig. 2c).

The morphology and the evolution of submarine canyons are sensitive to climate and sea level change, bottom current, and tectonic processes (Harishidayat et al., 2024). Yet, submarine canyons around the world share similar thalweg (valley floor) and shelf depths at their shoreward terminus (about 150 m vs. 20 m depth, respectively). Similar features in the wave-field may therefore be expected, especially the upper frequency cut-off for reflection of waves, which is mainly controlled by the depth-contrast. For instance, at the La Jolla and Scripps canyons which were studied during the Nearshore Canyon Experiment (NCEX) the cut-off frequency for the reflection of swell appear to be around 7—9 seconds period (Munk and Traylor, 1947; Magne et al., 2007). Most of the studies resulting from NCEX focused primarily on infra-gravity waves (where the width of the canyon is more important for the reflection and transmission of waves) (Douglas, 2004; Thomson et al., 2005, 2007), except Magne et al. (2007) who looked at the broader wave spectrum including swell, as we are doing here. In our study we have far greater spatial and temporal resolution of the measurements, so that we can study the short-term variations of in the wave field and the gradient across the canyon edge. We are therefore able to distinguish the effect of the canyon geometry more clearly, which appears to cause more focusing at Nazaré compared to at the La Jolla and Scripps-canyons.

The oceanographic and geological environment of the Nazaré Submarine Canyon

The Nazaré canyon extends about 210 km westward from Nazaré to depths greater than 4500 m, and is characterized by steep slopes, terraces, scarps, and a deeply incised *thalweg* in its lower section (Tyler et al., 2009). The canyon originates from a complicated history of different processes active for different periods. Faults related to the tectonic plates are responsible for controlling the geomorphology of parts of the canyon. These are still active and connected to the same system of faults, in which the 1755 Lisbon earthquake occurred.

The currents, the shape of the canyon, and the erosion of the beach and canyon are connected to the waves. Mostly, these factors affect the waves, but over time the waves may also influence their environment. The main environmental factors are therefore briefly described here: Just north of the town of Nazaré, a promontory extends from the coast (composed of hard

https://doi.org/10.5194/egusphere-2026-2778
Preprint. Discussion started: 1 June 2026

Cretaceous limestone, Cunha and Gouveia (2015)) with a 16th century fort and lighthouse, the *Forte de S. Miguel Arcanjo*. Beaches extend north (*Praia do Norte*) and south of the promontory. West, towards the sea from the promontory stands a stack of rocks known as *Pedra do Guilhim* (Guilhim rocks). This area is a popular fishing spot, while Praia do Norte is among the most famous surf spots in the world.

The submarine Nazaré canyon (Fig. 2a) acts as a sedimentary sink and captures the along-shore dominant sediment drift from north to south. Silva et al. (2013) observed that the coastline along the Praia do Norte (the North Beach) appears to oscillate throughout the year with the varying wave direction. The dominant wind directions are from north-west and south-west quadrants (Campos and Guedes Soares, 2018). Northerly wind and small waves cause the beach to become linear, while more westerly swell deposits sediments at the center of the beach and causes it to become curved. Waves and wave-breaking drive currents and eddies along the beach (Baker et al., 2021), and shape beaches and generate beach cusps (Dalrymple and Lanan, 1976). A similar process is observed at La Jolla, California where wave refraction induced by a submarine canyon was linked to patterns of localized beach erosion, driven by the focusing of wave energy onto specific stretches of the shoreline (Munk and Traylor, 1947).

Looking eastwards from the coast, the part of the canyon that cuts through the continental shelf is described as the *upper canyon*, it runs in the west-southwest direction towards the North Atlantic Ocean. In this part of the canyon, the thalweg is less than 100 m wide. The continental shelf extends about 20 to 60 km westward from Portugal down to a depth of about 200 m, where the slope of the seafloor steepens to $6°$. The canyon is not connected to a river system, but is still a major pathway for sediment transport in the region. Above 300 m depth, the northerly wind causes a southward flow across the shelf, generating flow upwards the canyon. In the absence of northerly winds, the flow is mainly down-slope in the canyon. The canyon disturbs the predominant north-south circulation (parallel to the continental shelf) significantly, with strong meandering currents aligned along the axis of the canyon.

In the upper canyon, which is where this study is focused, the lunar semi-diurnal tide causes internal waves to propagate upward the canyon where they are reflected. The tidal process and the reflections cause intermittent high bottom currents (up to 70 cm s^{-1}) down-slope (Tyler et al., 2009). The canyon terminus is about 200 meters west of the lighthouse (150 meters south of the lighthouse), where the shelf is about 12 meters deep. At about 660 meters from the lighthouse along the canyon axis, at a depth of 21 meters, the northern canyon edge makes a distinct turn from a south-westerly direction to a more westerly direction. And at 912 meters, where the depth is about 30 meters, it makes a further turn towards the west. The bearing of the canyon edge between the first turn (Fig. 2a) and the lighthouse is about $48°$ (*segment 1*), the bearing of the canyon edge from the second turn towards the first turn is about $71°$ (*segment 2*). Outside that the bearing of the canyon edge is about $86°$ (*segment 3*), before curving slightly towards the south and west again. The slope of the shelf towards the canyon edge is about $2.4°$ downwards, before reaching the canyon edge where the slope quickly steepens to about $60°$ downwards over 20 meters (steepest in segment 1 and segment 3, Fig. 2a).

https://doi.org/10.5194/egusphere-2026-2778
Preprint. Discussion started: 1 June 2026

2 Wave propagation at the Nazaré submarine canyon

Waves arriving from the west to north-west sectors propagate onto the continental shelf towards Nazaré and encounter the northern canyon edge. As the depth increases the phase speed also increases (see e.g. Holthuijsen (2007)). At Nazaré the gradually sloping sea-floor towards the canyon edge (Figure 3) will cause the waves to refract towards the area of lower wave-speed and thus effectively increase the incidence angle of the wave components before they reach the steep cliffs. The steep cliffs towards the thalweg are more accurately described as partial or complete reflections of the waves. Since the phase speed is dependent on the depth, the refraction and reflection are also dependent on wave period. Longer waves will therefore be more strongly refracted and reflected (unless they are long enough to be transmitted, Thomson et al. (2005)), while shorter waves are less affected by the change of water depth below.

At Nazaré the effect of the canyon of the incident wave field can broadly be described by refraction and reflection. We therefore attempt to explain the phenomena using two wave models, a ray tracer (refraction, Halsne et al. (2023b)) and a Boundary Element Method (reflection, Hope et al. (2026)). Spectral wave models, like WAVEWATCH III or SWAN (The WAVEWATCH III R © Development Group (WW3DG), 2019; Booij et al., 1999), are not suitable in explaining these phenomena, because the wave field is, at least to a large degree, a result of coherent interference, requiring the phase of the waves to be modeled. As the water depth decreases, the wave amplitude increases due to shoaling (see e.g. Kinsman (1965)). In this study, the longest waves observed were about 13 seconds longs. At 10 m depth, the shoaling coefficient for this period is 1.03. For a wave period of 20 seconds, the shoaling coefficient at 10, 15, and 20 meters would be 1.26, 1.14, and 1.07, respectively . The depth at the canyon edge is between 20 and 15 meters at the shallowest. The change in amplitude in this area is therefore most likely affected by the superposition of refracted and reflected waves, and not by shoaling. As the waves approach the beach, the shoaling becomes the dominant factor in amplifying the wave height.

Waves encountering an abrupt change in water depth, where the change is comparable or smaller than the wave length, are better described as reflected rather than refracted. The waves are often approximated as an incident, transmitted, and reflected field of plane waves with constant coefficients (Kirby and Dalrymple, 1983; Raichlen and Lee, 1978). The reflection and transmission coefficients are defined as

$$T = \frac{a_t}{a_i} \tag{1}$$

$$R = \frac{a_r}{a_i}. \tag{2}$$

The coefficients of reflection and transmission due to bathymetry are generally not trivial to estimate (Elga, 1994; Feddersen et al., 2003). Thomson et al. (2005, 2007) computed the coefficients for infra-gravity waves across the entire La Jolla and Scripps canyons. If the width of the canyon is small compared to the wave length, more energy is transmitted across the canyon (Thomson et al., 2005) while long waves may also be trapped in the canyon (Ray et al., 2022). For swell, however, the wave length is significantly shorter than the canyon width, and the reflection from the canyon edges can be independently considered. Therefore we consider the long-wave approximation less appropriate in this study (small kh, and equivalent to Lamb (1932)

https://doi.org/10.5194/egusphere-2026-2778
Preprint. Discussion started: 1 June 2026

§176) used by Thomson et al. (2005), since we are studying waves of period $T \lesssim 20$ s. Magne et al. (2007) compares several different methods to compute the reflection coefficient in the same canyons for shorter waves. We take a similar approach, using the plane-wave approximation (*PWA*) in Kirby and Dalrymple (1983) (Eqs. 4.4a and b therein). The reflection coefficient is calculated for a symmetric trench: With the shelf depth set to $h_1 = h_3 = 20$ m, the canyon depth is set to $h_2 = 150$ m, and the canyon width is set to $L = 250$ m with a ratio $h_2/h_1 = 7.5$ so that the *PWA* method is valid.

Waves traveling from the shelf to deeper water will have a higher phase speed when they are above the deep water. For increasingly steeper angles of incidence the cross-canyon wave number eventually becomes imaginary (total internal reflection). In Figure 4a the contour of where the cross-canyon wave number is imaginary (critical angle) is shown as a function of the incident angle and period. For periods above 7.5 s, the cross-canyon wavenumber is imaginary for incident angles above $60°$. Above this contour, we expect total internal reflection (assuming that the wave length is short compared to the canyon width, so that there is no energy leaking across the canyon). In this case, the reflection coefficient is 1, and the transmission coefficient should be reinterpreted as the non-propagating evanescent wave (Kirby and Dalrymple, 1983). As can be seen in Figure 4a, waves with a large incidence angle are completely reflected due to total internal reflection. This was observed by Magne et al. (2007) for swell at La Jolla and Scripps which often arrive from directions above the critical angle, and were generally totally reflected.

Figure 4b shows the reflection coefficient for waves coming from incident onto the edge depending on the edge bearing. Assuming the majority of swell arrives from $300°$ (Fig. 1), for the outermost part of the edge ($86°$, see Sec. 1 and Fig. 2a) the cut-off wave-period for almost total reflection is about 9.6 seconds, longer waves are completely reflected. For the middle segment (between the two turns), the cut-off wave-period is 11 seconds. For the innermost segment waves arriving from $300°$ and further north is mostly transmitted through, waves coming from further south are completely reflected when longer than 9 seconds.

2.1 Modeling setup

Two methods of modeling the wave-field are applied: ray tracing (Halsne et al., 2023b) and the Boundary Element Method (BEM) (Hope et al., 2026; Kirkup, 1998, 2019). The ray tracing captures the effect of refraction due to the phase-speed change caused by the bathymetry. By binning the rays on a grid to calculate their density, incoherent focusing is estimated. The BEM-model is used to represent the reflection from the complex geometry of the canyon edge. A boundary is set along the 50 m contour, encapsulating the canyon rim in the horizontal plane, and bounding it on the western end at a depth where swell is not affected by the shelf. The boundary consists of 683 linear segments of approximately 30 m length, interpolated along the 50 m depth contour. The BEM-model can calculate the phase-resolved interference pattern caused by the canyon edge, which can then be superimposed on a source field. Each wavenumber component for plane waves are calculated independently. Along the boundary the reflection coefficient as calculated above (Fig. 4a) is multiplied with the incoming plane wave. An attenuation of $\mu = 3.7 \times 10^{-7}$ $[\mathrm{m}^{-1}]$ (Ardhuin et al., 2009; Collard et al., 2009; Jiang et al., 2016) is used to parameterize dissipation of short waves. This value (derived for swell propagating long distances) is uncertain, but it is used as an approximation of the

https://doi.org/10.5194/egusphere-2026-2778
Preprint. Discussion started: 1 June 2026

dissipation or lack of coherence that would otherwise cause unrealistic interference patterns and far away from the boundary, and the area of interest.

The goal is to study the interference pattern close to the boundary, the reflected and incident field of each wavenumber component is therefore superimposed coherently (retaining the phase) into the total field for a given wavenumber component. However, further away from the boundary this assumption quickly breaks down, depending on the crest length of incoming plane wave. Further, the total fields (reflected and incident) for each wavenumber component are summed incoherently, to avoid making too strong assumptions about the stability of phase, accuracy of the method, and crest lengths:

$$\mathrm{Var}(\phi_t) = \sum_i \mathrm{Var}(\phi_i) \tag{3}$$

where ϕ_i is the total field (incident and reflected coherently summed) for wavenumber component i, and the sum is over all wavenumber components. The variance of a single harmonic wave ϕ_i, with amplitude Φ_i is: $\mathrm{Var}(\phi_i) = \sigma_\phi^2 = \frac{1}{2}\Phi_i^2$ (Holthuijsen, 2007, Ch. 3.5). For an incoming field, I, the spectral transfer function and the magnitude of the amplitude transfer function (Holthuijsen, 2007, Ch. 3.5 and 3.6) are calculated as:

$I + R \cdot I$ for waves originating north of the canyon edge

$T \cdot I$ for waves originating south of the canyon edge

This way, two dimensional energy spectra may be multiplied with the computed transfer function to determine the spectrum at points closed to the shore. Or when retaining phase-information, typically with single wavenumber components, the amplitude and phase may be calculated for points close to the shore. By superimposing reflected and incident field within each wavenumber component coherently, and incoherently across wavenumbers, the interference pattern with partial coherence is computed. Both models use the EMODnet digital bathymetry (EMODnet Bathymetry Consortium, 2022).

3 Experiment and model results

Two experiment setups were used: one looking westwards along the canyon edge (Fig. 2b), and one looking towards the north (along the beach, Fig. 2e). The first setup was repeated twice. Arrays of small wave-buoys (Hope et al. (2025), Fig. 2d) were deployed using JetSkis in a cross-pattern so that they would drift across the canyon edge. The buoys drifted through the field-of-view of the cameras, so that the wave-field was measured using the two methods simultaneously.

The wave buoys shown in Figure 2d track their GPS position every 5 seconds and sample the acceleration of the sea surface at 52 Hz. Acceleration is integrated twice to obtain elevation. The buoy is designed to be lightweight, and is contained in an 800 ml bottle and weighs about 0.5 kg. The JetSki could therefore carry about 10 buoys at once. The high sample rate and continuous time-series allow us to track the phases of waves and detect breaking waves. However, in order to truly match the phase and location between the buoys more accurate GPS positioning and timing is required. The buoys are too small to be visible to the camera at this distance, therefore control points in the field of view of the cameras are established when the buoys

https://doi.org/10.5194/egusphere-2026-2778
Preprint. Discussion started: 1 June 2026

are deployed from the JetSki. The drift of the buoys is dependent on wind, currents, and to the waves. Predicting where the buoys will drift was therefore not easy to do in advance.

Because the wave conditions were relatively mellow, and the wind would sometimes push the buoys offshore, we were able to recover almost all the buoys after each experiment. However, some where lost when crushed against the cliffs or when they drifted too close to the cliffs for the JetSki to safely recover them. The buoys therefore transmitted its data (full time-series) every 10 minutes so that only a limited amount of data would be lost. Additionally, the buoy stored the data to a SD-card so that if it was out of cell range (too close to the cliff), or too frequently submerged (caught in continuously breaking waves), the data could also be recovered with the buoy.

The stereo video setup consisted of a pair of synchronized JAI GO-X 16205-PGE cameras equipped with 1.1" Sony IMX542 Pregius CMOS sensor. They were set to record 4 frames per second with a spatial resolution of 5328×3040 pixels. The lenses are industrial KOWA 8.5mm $f/16$ focal length lenses focused at infinity. Synchronized image pairs were used to reconstruct the ocean surface $\eta(x, y, t)$ using WASS (Bergamasco et al., 2017). The cameras were mounted in similar configuration to Benetazzo (2006); Guimarães et al. (2020); Vieira et al. (2025). The steep coastal cliff improves the aspect, and the cameras produce useful data over the first part of the canyon edge. However, the furthest buoys are outside of the reliable area measured by the cameras. The cameras were placed 6.19 m apart, with an inclination of $70°$. The distance to the ocean was 250 — 550 m and 100 — 700 m when overlooking the canyon and the beach, respectively. Their altitude above the mean water level is 50 m.

3.1 Wave-conditions

Two types of wave-conditions were measured, with a total of three experiments conducted in the refraction zone, the area covering both the shelf, the edge and the deep canyon close to the shore. Although the waves were not particularly large, their periods were sufficiently long to undergo refraction. During the second experiment, the wave-conditions promoted breaking waves up to 7 meters in height. In two of the experiments, the stereo-camera system covered the same area as the wave buoys within its field of view. For each experiment ray-tracing and BEM-modeling is performed in order to interpret the results and evaluate the models.

Figure 5 show the general wave conditions throughout the week of experiments. Two wave buoys were deployed on Tuesday 4th of November 2024 and drifted north along the coast. They generally maintain a distance of around 10 km from the coast and thus provide a measure of the incoming wave field. As can be seen in Figure 5, they match well with the significant wave heights forecasted by *ECMWF*. Occasionally, the buoys report exaggerated and noisy wave heights. These are likely caused by the buoys drifting into the breaking waves temporarily. As the buoys drift northward they become less relevant to the wave conditions outside Nazaré.

Measurements taken over shorter time windows throughout the week are shown as points, which also match very well with the forecasted wave heights and spectra.

https://doi.org/10.5194/egusphere-2026-2778
Preprint. Discussion started: 1 June 2026

3.2 Waves incident almost along the canyon axis (from west-south-west sector)

Figure 5b show the forecasted spectrum for Tuesday 5th November 2024 at 13:00. The peak wave direction travel almost along the canyon axis, slightly from the north. Figure 6 show the measured spectra and the drift directions for the two deployments made. In the first the buoys only drifted above the canyon (Fig. 6a), while in the second deployment the array drifted from above the canyon and above the shelf towards the beach (Fig. 6c).

The forecasted 1D spectrum is plotted together with the measured spectra. The outermost buoy (*49*) shows the best agreement with the forecasted wave spectrum (Fig. 6b and 6d). Over about 20 minutes the buoys drift towards the North-beach and through the breaking waves. At this point the buoys have passed through the focus zone, and into the breaking waves. The measured wave field is therefore not stationary over the spatial distance the buoys are traveling, and the full-time spectrum is not very trustworthy.

To capture the evolution of the wave field a spectrogram is calculated for each buoy and shown in Figure 7. The spectrogram is constructed from the Short-Time Fourier Transform (STFT) from the elevation time series. A window length of 4096 samples with 50% overlap (FFT size of 8192) is used, corresponding to a window length of 79 seconds. Each STFT is scaled to the Power Spectral Density (PSD) so that it shows the elevation variance density as for a traditional wave spectrum. The water-depth underneath the buoy is also plotted, as well as the rolling-window variance (m_0, window size 8192). For reference, the peak period is plotted as a constant horizontal line.

For the first drift the buoys are located only above the shelf (Fig. 6a) and the low-frequency waves are present most of the time. Eventually the buoys drift into the breaking waves, and impulsive events are observed towards the end of the time series (Brown et al., 2018; Brown and Paasch, 2021). These events result in low-frequency noise in the spectrum covering the entire drift (Fig. 6b), as discussed in Hope et al. (2025). In the second drift, the buoys were deployed above the canyon and drifted northwards above the edge towards the beach (Fig. 6c). The spectrograms shown in Figure 6d show that the buoys measure very low energy above the canyon. However, as the buoys approach the edge of the canyon and drift onto the shelf the low-frequency energy seen in the first drift re-appears. The variance is low above the canyon. In both drifts, the variance oscillates above the shelf, as the buoy is drifting north-east.

The full-time spectra for the buoys that spent most time above the canyon, compared to those that spent more time above the shelf, appear to have a cut-off of about 0.15 Hz, or 6.6 s, where the energy levels are similar. In the spectrograms (Fig. 6d), the frequencies above the same level also appear to be equally present along the whole transect. Most of the incoming energy is located in the lower frequencies, reducing the signal-to-noise ratio.

In order to compare the images from the stereo cameras with the time series measured by the buoys, three lines with virtual sample points are picked in the image. The points are shown along with the starting point (circle), and the distances from the starting points along the lines in the upper panel of Figure 9c. For each point a ten minute Welch spectrum is calculated (PSD). The spectra is plotted as a spectrogram as a function of the distance from the starting point in Figure 7c. The cross-canyon lines (upper two panels) start on the shelf and move above the steep drop (contours of bathymetry shown). The same pattern seen in the spectrograms recorded by the buoys (Figure 7b) is visible here: low frequency energy is only visible above the shelf.

https://doi.org/10.5194/egusphere-2026-2778
Preprint. Discussion started: 1 June 2026

Since the spectrogram computed for the stereo camera data show the same spatial distribution of low-frequency energy as the (short-time)-spatial spectrogram computed from the drifting buoys, the change in energy from above the canyon and onto the shelf is not due to temporal variability (non-stationarity) in the wave field. The stereo-video spectrum is calculated for a longer time period in each point, this explains a somewhat greater variance than what is observed for the buoys (which are computed for a shorter time window in order to be representative of a single point).

3.2.1 Model and comparison with data

Initially, we expected the buoys and cameras to measure swell above the canyon since the wave direction is almost the same direction as the canyon axis. However, the data showed that the swell components of the spectrum were very low above the canyon (Fig. 7b and 7c). Ray tracing (Figure 8) reveals a shadow zone where the canyon makes a northward turn west of the lighthouse (first turn in Fig. 2a). The shadow zone match the absence of swell. However, on the shelf, north of the canyon, the rays continue to be more or less unperturbed. In addition, the energy that is continuously refracted onto the shelf is propagated north-northeast from the canyon edge. Therefore, we observe a strong component of swell with long periods at this location (Figure 6b).

The interference pattern of incident and refracted or reflected waves is responsible for the focusing. Since the ray-tracing shows that the shape of the canyon edge is essential to the wave propagation, the complex geometry of the canyon must be accounted for when calculating the wave-field. In Figure 9 the Boundary Element Method is used together with the reflection coefficient for a step in the bathymetry (Fig. 4a). The boundary is placed along the 50-meter contour.

Figure 9a shows the amplitude response for a single wave component, namely the peak period (Fig. 5b). This gives an impression of the interference pattern of the incident waves superposed on the reflected field. It is clear that altering the boundary, or changing to a slightly different phase shift in the complex reflection coefficient, will cause the highs and lows to be shifted spatially. A stable interference pattern is dependent on a long enough crest length that the same wave can be considered to intersect with its reflection. This is true only for a limited distance from the boundary. Between wave components the accuracy of the input and the simulation (simplified to a reflecting boundary) no longer makes sense to assess coherently.

A more robust way is to sum each wave component coherently, and sum all the wave-components together incoherently so that we have an estimate for the spectrum response. The spectrum response can be multiplied with the directional spectrum (from ECMWF, e.g. Fig. 5b) to propagate the offshore spectrum to the area around the canyon edge. Figure 9b shows the variance and the areas where the incident and reflected field increase the intensity in the wave-field. The wave-field is only calculated for the exterior domain, outside the canyon.

Figure 9c compares the 20-minute measured variance by the stereo-cameras with the calculated amplitude response (peak period) and the calculated total field (variance, Fig. 9c). The tracks from the buoys (Fig. 6c and 6d) are shown, as well as the contours of the canyon bathymetry. Just north of the canyon the energy is higher where the reflection constructively interfere with the incident field. The BEM model predicts oscillating beams in the peak period.

https://doi.org/10.5194/egusphere-2026-2778
Preprint. Discussion started: 1 June 2026

3.3 Waves obliquely incident to the canyon axis (from north-west sector)

On Friday the 8th of November 2024, the waves arrived from the north-west (Figure 5c). They encounter the northern canyon edge at an oblique angle. Towards the shoreline, as the canyon turns towards the north, the peak direction is almost perpendicular to the canyon edge. Waves arriving from the north-side of the canyon edge will mostly be reflected (or refracted to the point of total internal reflection). However, when the incident angle turns towards perpendicular incidence, and the along-canyon wave-number decreases, the waves will eventually be transmitted across the edge and the canyon (Fig. 4b).

On this day, the stereo-cameras were pointed towards the north, in the direction parallel with the beach. They measured the area where the waves are focused towards the beach. The buoys were released above the canyon and drift further above the canyon along the easternmost terminus of the canyon. Their drift path and full-time spectra are shown in Figure 10. The spectra measured by the buoys are significantly lower than the forecasted offshore spectrum. The buoys drift with a speed of 0.20 to 0.25 m/s (slow compared to the phase-speed, so that the Doppler-shift is negligible).

The innermost buoys start their drift just west of the Guilhim rocks, drifting along the edge and along the edge of the canyon terminus, towards the south-east. The buoys further out stay primarily above the canyon, but all cross a ridge extending from the shelf and into the canyon. All buoys show higher energy here above the ridge, also at lower frequencies (Figure 11a, calculated as in Sec. 3.2). The variance (m_0), calculated using a rolling window, is shown as a red-line in Figure 11a. It generally correlates positively with the depth below the buoy (white line), but oscillates in peaks along the drift-path, suggesting that there may be an interference pattern or smaller scale focusing along the canyon edge and the shelf along the canyon terminus towards the south. Since there is little low-frequency waves measured by the buoys further out, the waves must either be propagating along the shelf around the canyon terminus. Alternatively, they may result from a part of the wave-field encountering segments of the canyon edge at an almost perpendicular angle, and thus passing through and onto the terminus of the canyon. Above the canyon, close to the canyon edge, the buoys should be in the evanescent, non-propagating, part of the reflected wave-field.

The buoys all measure a mean wave period (T_{m02}) of about 7 seconds (Fig. 10b). There is energy at lower frequencies as well, but it is significantly muted compared to the incoming wave-field. Since most of the incoming energy is below the anticipated cut-off frequency, the exact cut-off frequency is difficult to pinpoint accurately.

The virtual sample points (Fig. 11b) show that the first cross beach line (orange) perpendicular to the beach (closest to the cameras) is in an area of less variance, while the second cross beach line (green) shows higher variance. The along-shore line (blue) shows the dip in energy where the first line (cross beach 1) is placed. These high variance areas are interpreted to be beams of focused waves onto the beach.

3.3.1 Model and comparison with data

The energy-carrying waves (13.51 s, 11.84 s) of the incoming spectrum are selected and traced as rays. The rays are shown in Figure 12a.

The rays approach from the north-northwest and are initially refracted towards the shore (leftward of the ray) due to the slightly uphill bathymetry towards the canyon edge (Fig. 3). The initial refraction increases the incidence angle at the canyon

https://doi.org/10.5194/egusphere-2026-2778
Preprint. Discussion started: 1 June 2026

edge (Fig. 4b), and thus alters the reflection or refraction here. As the rays encounter the steep canyon edge, they are strongly refracted. Where the canyon makes a northward turn, some rays encounter the edge more perpendicularly and are transmitted into the canyon. There is a shadow-zone in the same area as seen for waves arriving along the canyon axis (Sec. 3.2).

The rays that escape through the canyon edge, towards the lighthouse, where the buoys drifted past, may explain why low-frequency energy is seen here. The ray density (Fig. 12b) indicates that the energy is focused towards the beach north of the canyon, and that for the longer periods there is a secondary peak further north (left-most panel). In Figure 13 the interference patterns are calculated using the BEM model. Several beams are visible in addition to a focus just north of the canyon. The BEM model does not take into account the refraction that occurs before or after the waves encounter the canyon edge.

In Figure 13, the peak wave component and the full 2D forecasted spectrum from ECMWF modeled using the BEM above the canyon is shown. In Figure 13c and 13d the BEM model is compared to the measured variance by the stereo cameras. In both we see a pattern of beams extending towards the beach. The BEM model does not account for refraction due to the shallower water before the beach, and the waves are therefore not bent towards the beach. Note that the scale between modeled and measured variance is comparable, but not equal. A photo taken at the same time towards the north (Fig. 13e) shows gaps in the waves in the along-beach direction. The same pattern is seen in the reconstructed sea-surface from the stereo-cameras (Fig. 13f), where the wave peaks are formed along the beams separated by the gaps seen in the variance and BEM-modeling.

3.4 General wave propagation and optimal focusing

In Figure 14 BEM and ray-tracing simulations for different wave periods and directions are shown. The amplitude is shown on the left panel, followed by the variance of the reflected field and the variance of the (coherently) superimposed incident and reflected fields.

Waves traveling towards between $75°$ (from $255°$, top row in Fig. 14) and $125°$ (from $305°$, bottom row in Fig. 14) cause particularly strong focusing towards the beach. This is slightly on the edge of the predominant direction for which waves arrive from (Fig. 1). The BEM model shows that the greatest focusing of happen when waves arrive from about $270°$. Waves shorter than about 7 seconds are not refracted enough to be focused, and largely cross the edge of the canyon (third row in Fig. 14). The same is true for longer waves arriving more steeply (low angle of incidence) from the north (towards about $125°$, bottom panel), their along-canyon wavenumber is low enough that they also pass through without significant focusing, and only the longest waves are somewhat reflected and refracted at the canyon edge (Fig. 4a and 4b)

The angle of incidence and the frequency modulates the interference pattern onto the beach, with distinct beams of higher energy. Waves arriving from a more southerly direction the beams to be more compacted towards the lighthouse. Increasing the frequency also compacts the beams, before they are reduced. The main beams (closest to the canyon edge) and its side-lobes towards the north may explain the secondary and tertiary *peaks* known to the surfer community.

Importantly, the BEM model does not account for the counter-clockwise refraction of wave rays and the subsequent increase in incidence angle by $5° — 15°$, caused by the upward-sloping shelf before the canyon edge (Fig. 3). Therefore, the directions causing the maximum focusing should be waves traveling towards about $95°$ to $135°$, or waves arriving from between about $275°$ to $315°$. In the surfer community, waves arriving from around $290°$ to $315°$ are usually considered to produce large waves.

https://doi.org/10.5194/egusphere-2026-2778
Preprint. Discussion started: 1 June 2026

Reflections from the canyon edge further west may be exaggerated since the depth of the shelf in the BEM model is fixed at 20 meters.

4 Discussion

4.1 Wave propagation and reflection at the edge of the canyon

The large waves at Nazaré are commonly explained as being channeled up the canyon. The incident direction of the waves arriving along the canyon axis (Fig. 5b) arrives on the south-side of the north-canyon edge on the outer parts of the canyon, but on the north-side of the canyon on the inner sections where the canyon turns northwards (Fig. 4b). If the waves were refracted or focused along the canyon, we would expect the entire canyon to be illuminated by the incoming wavefield. However, both the measurements from the buoys and the stereo-cameras show that long period waves are significantly muted above the canyon (close to the north-edge).

Ray-tracing shown in Figure 8 show a clear shadow-zone above the canyon, where the canyon turns towards the north (close to the promontory). It is therefore clear that *(1) the waves are not channeled in the canyon*, but are shaped by the canyon edge. And, *(2) the wave-field is sensitive to the geometry of the canyon edge*.

Waves propagating from the north-west above the shallower continental shelf encounter the canyon edge. Above the shelf the phase speed is slower, and above the canyon the phase speed is greater, so that the waves are refracted or reflected at the edge. Where the canyon edge turns towards the north closer to shore some waves may pass through above the canyon. A satellite image from 2023 illustrates the reflection clearly in Figure 15. The simulated rays show how the reflection follow the northern edge of the canyon and focuses the energy towards the northern beach. In particular, they cannot be channeled by the canyon further out, since the shelf is too deep to refract the waves. Waves arriving along the canyon axis appear to be scattered northwards by the canyon edge, and are (1) not focused strongly towards the beach, and (2) do not have an incoming field to constructively interfere with.

The shelf drops slightly towards the canyon edge, resulting in counter-clockwise refraction of the waves arriving from the north of the canyon. This causes an increased incidence angle as the waves encounter the canyon edge, causing the waves to be more strongly refracted (Fig. 3) or reflected (Fig. 4a). For waves arriving from the west this may reduce focusing, since the waves are refracted too strongly and defocused along the canyon edge. While waves from more north-northwesterly directions which would otherwise pass through, or unfavorably reflect, are focused more strongly.

In these experiments we measured two distinct wave conditions, and used two models, a ray tracer and a boundary element method, to extrapolate to other conditions. The models show significant focusing in the form of beams, which is recognizable in the data. Our results show that the amplitude change at T_p is primarily due to refraction, and not shoaling, since (1) the shoaling coefficient is very small in the measured area, and (2) the forecasted spectrum agrees well with those measured by the buoys on the shelf (before the buoys enter the breaking waves).

https://doi.org/10.5194/egusphere-2026-2778
Preprint. Discussion started: 1 June 2026

The large wave generation at Nazaré is therefore most accurately explained as being primarily refracted and reflected into focused beams within the final hundreds of meters along the northern edge of the canyon. The reflection happens at the northern edge of the canyon, and the curved shape of the canyon edge cause greater focusing than a straight or convex edge would.

Modeling suggest that similar turns or features in the canyon further out may focus energy into beams further north along the beach as well. This may explain the secondary and tertiary *peaks* utilized by the surfing community. The beams' locations in space are dependent on wave direction and wave period. The stereo camera captures features that qualitatively match the pattern of the predicted beams. However, the spatial placement of the beams is offset between the measurements and the model. The placement and shape of the interference pattern is dependent on where the boundary is placed in the BEM model, the phase shift from the reflection coefficient, water depth (tides, sea-bed morphology), and the accuracy of the offshore modeled input spectrum.

The waves drive the near-shore current and near-shore transport (Baker et al., 2021; Tyler et al., 2009), and is responsible for changes in the beach throughout the year. Winter conditions, when waves are greater, result in a beach that is curved (arcuate) (Silva et al., 2013). The current also affects the wave-propagation (Gallet and Young, 2014; Halsne et al., 2023a), and it may also be a secondary factor, in addition to the bathymetry, in the wave propagation. We have not taken into account changes in depth following the passage of the tides. The bathymetry, in particular close to the rocks where it may be difficult to measure safely, also has uncertainties.

4.2 Modeling of refraction and reflection

In this study we use two methods for modeling the wave propagation, a high frequency approximation (ray-tracing), and a full wave model (linear waves, BEM) with a sharp reflecting boundary. The reflective boundary is coupled with the modeled reflection coefficients for a step in the bathymetry (Kirby and Dalrymple, 1983). The motivation for using a full wave model is to study the interference pattern, which is not directly available through ray-tracing methods. The main disadvantage of the BEM in this work is that the simulated field is sensitive to the exact placement of the boundary and the amplitude and phase shift of the reflection coefficient.

A combination of both refraction and a reflective interface using, e.g., the Kirchoff method (Frazer and Sinton, 1984), as well as the reflection coefficients would be an interesting further step. Either a ray-tracer with support for reflective interfaces, as in, e.g., Thomson et al. (2007), or a more advanced model capable of handling non-linear wave propagation, like REEF3D or similar (Bihs and Wang, 2025). The advantage of the approach taken here, i.e., combining a BEM (including reflections from abrupt depth changes) with ray tracing, is that many wave conditions can be computed quickly and a linear transfer functions can be computed in advance. The transfer function can later be multiplied with a forecasted or measured offshore directional spectrum to obtain the wave field close to the shore.

https://doi.org/10.5194/egusphere-2026-2778
Preprint. Discussion started: 1 June 2026

5 Conclusions

Swell arriving at the North beach (Praia do Norte) outside Nazaré is refracted and reflected by the canyon edge. We find that the waves that yield the greatest focusing and the highest surf originate on the north side of the canyon and are not channeled through the canyon, as is commonly stated, before propagating across the shelf. The shelf slopes slightly downwards at an angle of $2.4°$ towards the canyon edge, causing the waves to be refracted counter-clockwise before reaching the canyon edge, increasing the incidence angle onto the canyon. The canyon wall steepens to a cliff so steep ($60°$) and deep that the waves are mostly reflected (modeled using reflection coefficients, Fig. 4a, Kirby and Dalrymple (1983)), as opposed to refraction which Magne et al. (2007) observed to be dominant across the Scripps-canyon. Further studies should be performed to determine the cause of these opposing results. Waves shorter than about 7 seconds, or waves hitting the canyon edge at nearly perpendicular angles, pass through. This is similar to the Scripps-canyon (Magne et al. (2007) and Fig. 13 therein), and given that many canyons around the world have similar thalweg-depths, a cut-off frequency of about 0.14 Hz may be common to many submarine canyons.

In this study, stereo cameras were mounted at the fort looking first along the canyon axis, and then towards the North beach where the greatest focusing occur. Simultaneously, arrays of light-weight wave buoys were deployed using a JetSki in a cross pattern so that they sample both the shelf and the canyon while drifting. Their light weight allowed many to be deployed simultaneously by the small craft (Cavaleri et al., 2025).

Two sets of wave conditions were measured: waves arriving almost along the canyon axis, and waves arriving obliquely, almost perpendicular, to the canyon edge on the northern side. In general, at Nazaré, swell arrive mostly from a sector around $300°$ (NNW, Fig. 1). A ray tracer and BEM model were compared to the measured data and used to extrapolate to general conditions. Since the models are efficient to run, the transfer function and response spectrum can be calculated. These may be multiplied with an arbitrary input spectrum to obtain the spectrum or the wave field close to the coast. The models show maximum focusing of waves arriving from about $275° — 315°$, while the surfing community normally considers waves arriving about $290° — 315°$ to give the best conditions.

Both the model and the data suggest that the shape of the northern canyon edge is crucial for how the wave energy focused into beams towards the North beach. Particularly, the northwards turn of the canyon in the final hundreds of meters. For swell, the last hundreds of meters (approximately $650 — 900$ meters) of the canyon is responsible for the refraction and reflection at the North beach. Further out towards the sea, the shelf is deeper and does not reflect the waves strongly. However, the shape of the edge outside the second turn (Fig. 2a) may explain the focusing further north on the beach. Additionally, the interference of the incident and reflected waves (and their focusing) responsible for the large waves must coherently interfere. This is more likely to occur systematically (and thus coherently) near the reflecting boundary, while the phases remain relatively stable, so that the reflected wave may overlap with the next incoming incident wave.

Since the focused waves consist of waves arriving from multiple directions, they take on the shape of pyramids. The multi directionality is perhaps also necessary for the waves to sustain themselves to a greater height before breaking, and therefore enabling the large face-height of breaking waves observed at Nazaré (McAllister et al., 2024).

https://doi.org/10.5194/egusphere-2026-2778
Preprint. Discussion started: 1 June 2026

Code and data availability. The buoy measurements and stereo-video measurements this study are available at https://github.com/gauteh/nazare-2024-data and https://thredds.met.no/thredds/catalog.html. The ray tracing code is available at https://github.com/hevgyrt/ocean_wave_tracing, and the BEM code is available at https://github.com/gauteh/ohbemn. Bathymetry is available from EMODnet (EMODnet Bathymetry Consortium, 2022).

Author contributions. Concept: GH, PA, AB, ØB, FB, MV ER. Data analysis: GH, MV, FB, AB, TH. Field work: GH, ER, TS, MV, FB, ØB, PA, AB, CB. Model and theory: GH, TH, ØB. Manuscript: GH, TH, MV, ØB, MV, AB, PA, TS, FB, CB, BF.

Competing interests. The authors declare that there are no competing interests.

Acknowledgements. The authors would like to acknowledge the support of Nazaré Municipality and Nazaré Qualifica for facilitating access to the lighthouse, and for providing accommodation and logistical assistance essential to the success of this experiment. *ECMWF* and *Jean Bidlot* are thanked for their aid in providing and preparing forecasted spectra for the experiment. *João de Macedo* and friends are thanked for providing and driving the JetSki expertly, this experiment would not be possible without them. They provided feedback and a reality-check that has been essential for grounding this study in the real world. This study is funded by the *BigWaveTracker* project granted by the Portuguese Foundation for Science and Technology (FCT contract 2022.08288.PTDC), and the Research Council of Norway grant *B-WAVES* (no. 344357). *Helge Bryhni, Roger Storvik, Ask Breivik* and *Trygve L. Søvik* are thanked for their help in preparing equipment. *Jim Thomson* is thanked for discussions prior to the experiment and supplementary drifters.

https://doi.org/10.5194/egusphere-2026-2778
Preprint. Discussion started: 1 June 2026

References

Ardhuin, F., Chapron, B., and Collard, F.: Observation of Swell Dissipation across Oceans, Geophysical Research Letters, 36, 2008GL037 030, https://doi.org/10.1029/2008GL037030, 2009.

Baker, C. M., Moulton, M., Raubenheimer, B., Elgar, S., and Kumar, N.: Modeled Three-Dimensional Currents and Eddies on an Alongshore-Variable Barred Beach, Journal of Geophysical Research: Oceans, 126, e2020JC016 899, https://doi.org/10.1029/2020JC016899, 2021.

Benetazzo, A.: Measurements of Short Water Waves Using Stereo Matched Image Sequences, Coastal Engineering, 53, 1013–1032, https://doi.org/10.1016/j.coastaleng.2006.06.012, 2006.

Bergamasco, F., Torsello, A., Sclavo, M., Barbariol, F., and Benetazzo, A.: WASS: An Open-Source Pipeline for 3D Stereo Reconstruction of Ocean Waves, Comput. Geosci., 107, 28–36, https://doi.org/10.1016/j.cageo.2017.07.001, 2017.

Bihs, H. and Wang, W. W.: Reef3d::Nhflow - a High-Performance Non-Hydrostatic Solver for Coastal Wave Propagation, Coastal Engineering, https://doi.org/10.2139/ssrn.5145387, 2025.

Booij, N., Ris, R. C., and Holthuijsen, L. H.: A Third-Generation Wave Model for Coastal Regions: 1. Model Description and Validation, Journal of Geophysical Research: Oceans, 104, 7649–7666, https://doi.org/10.1029/98JC02622, 1999.

Brown, A. and Paasch, R. K.: The Accelerations of a Wave Measurement Buoy Impacted by Breaking Waves in the Surf Zone, Journal of Marine Science and Engineering, 9, 214, https://doi.org/10.3390/jmse9020214, 2021.

Brown, A., Thomson, J., Ellenson, A., Rollano, F. T., Ozkan-Haller, H. T., and Haller, M. C.: Kinematics and Statistics of Breaking Waves Observed Using SWIFT Buoys, IEEE Journal of Oceanic Engineering, 44, 1011–1023, https://doi.org/10.1109/JOE.2018.2868335, 2018.

Campos, R. and Guedes Soares, C.: Spatial Distribution of Offshore Wind Statistics on the Coast of Portugal Using Regional Frequency Analysis, Renewable Energy, 123, 806–816, https://doi.org/10.1016/j.renene.2018.02.051, 2018.

Cavaleri, L., Alari, V., Benetazzo, A., Bjorkqvist, J.-V., Breivik, O., Davis, J., Hope, G., Kleven, A., Leirvik, F., Nordam, T., Rabault, J., Rainville, E. J., Rikka, S., Seldal, T. I., and Thomson, J.: More Room at the Top: How Small Buoys Help Reveal the Detailed Dynamics of the Air-Sea Interface, Bulletin of the American Meteorological Society, https://doi.org/10.1175/BAMS-D-24-0120.1, 2025.

Collard, F., Ardhuin, F., and Chapron, B.: Monitoring and Analysis of Ocean Swell Fields from Space: New Methods for Routine Observations, Journal of Geophysical Research: Oceans, 114, 2008JC005 215, https://doi.org/10.1029/2008JC005215, 2009.

Cunha, P. P. and Gouveia, M. P.: The Nazaré Coast, The Submarine Canyon and the Giant Wave - a Synthesis, 2015.

Dalrymple, R. A. and Lanan, G. A.: Beach Cusps Formed by Intersecting Waves, Geological Society of America Bulletin, 87, 57, https://doi.org/10.1130/0016-7606(1976)87<57:BCFBIW>2.0.CO;2, 1976.

Douglas, S.: Wave Refraction over Complex Nearshore Bathymetry, M.Sc., 2004.

Elga, S.: Reflection of Ocean Surface Gravity Waves from a Natural Beach, Journal of Physical Oceanography, 1994.

EMODnet Bathymetry Consortium: EMODnet Digital Bathymetry (DTM 2022), https://doi.org/10.12770/ff3aff8a-cff1-44a3-a2c8-1910bf109f85, 2022.

Feddersen, F., Gallagher, E., Guza, R., and Elgar, S.: The Drag Coefficient, Bottom Roughness, and Wave-Breaking in the Nearshore, Coastal Engineering, 48, 189–195, https://doi.org/10.1016/S0378-3839(03)00026-7, 2003.

Frazer, L. N. and Sinton, J. B.: A Kirchhoff Method for the Computation of Finite-Frequency Body Wave Synthetic Seismograms in Laterally Inhomogeneous Media, Geophysical Journal International, 78, 413–429, https://doi.org/10.1111/j.1365-246X.1984.tb01957.x, 1984.

Gallet, B. and Young, W. R.: Refraction of Swell by Surface Currents, Journal of Marine Research, 72, 105–126, https://doi.org/10.1357/002224014813758959, 2014.

https://doi.org/10.5194/egusphere-2026-2778
Preprint. Discussion started: 1 June 2026

Guimarães, P. V., Ardhuin, F., Bergamasco, F., Leckler, F., Filipot, J.-F., Shim, J.-S., Dulov, V., and Benetazzo, A.: A Data Set of Sea Surface Stereo Images to Resolve Space-Time Wave Fields, Scientific Data, 7, 145, https://doi.org/10.1038/s41597-020-0492-9, 2020.

Halsne, T., Benetazzo, A., Barbariol, F., Christensen, K. H., Carrasco, A., and Breivik, Ø.: Wave Modulation in a Strong Tidal Current and Its Impact on Extreme Waves, Journal of Physical Oceanography, https://doi.org/10.1175/JPO-D-23-0051.1, 2023a.

Halsne, T., Christensen, K. H., Hope, G., and Breivik, Ø.: Ocean Wave Tracing v.1: A Numerical Solver of the Wave Ray Equations for Ocean Waves on Variable Currents at Arbitrary Depths, Geoscientific Model Development, 16, 6515–6530, https://doi.org/10.5194/gmd-16-6515-2023, 2023b.

Harishidayat, D., Niyazi, Y., Stewart, H. A., Al-Shuhail, A., and Jamieson, A. J.: Submarine Canyon Development Controlled by Slope Failure and Oceanographic Process Interactions, Scientific Reports, 14, 18 486, https://doi.org/10.1038/s41598-024-69536-8, 2024.

Holthuijsen, L. H.: Waves in Oceanic and Coastal Waters, Cambridge University Press, 2007.

Hope, G., Seldal, T. I., Rabault, J., Bryhni, H. T., Bohlinger, P., Björkqvist, J.-V., Nordam, T., Kleven, A., Mostaani, A., Furevik, B. R., Hole, L. R., Storvik, R., and Breivik, Ø.: SFY – A Lightweight, High-Frequency and Phase-Resolving Wave-Buoy for Coastal Waters, Journal of Atmospheric and Oceanic Technology, pp. 133–154, https://doi.org/10.1175/JTECH-D-23-0170.1, 2025.

Hope, G., Bohlinger, P., Halsne, T., and Breivik, Ø.: OhBemn (Version 0.2): A Simple Boundary Element Method-model for Ocean Surface Waves, EGUsphere, pp. 1–29, https://doi.org/10.5194/egusphere-2026-1198, 2026.

Jiang, H., Stopa, J. E., Wang, H., Husson, R., Mouche, A., Chapron, B., and Chen, G.: Tracking the Attenuation and Nonbreaking Dissipation of Swells Using Altimeters, Journal of Geophysical Research: Oceans, 121, 1446–1458, https://doi.org/10.1002/2015JC011536, 2016.

Kinsman, B.: Wind Waves, 1965.

Kirby, J. T. and Dalrymple, R. A.: Propagation of Obliquely Incident Water Waves over a Trench, Journal of Fluid Mechanics, 133, 47–63, https://doi.org/10.1017/S0022112083001780, 1983.

Kirkup, S.: The Boundary Element Method in Acoustics: A Development in Fortran, no. 1 in Integral Equation Methods in Engineering, Integrated Sound Software, Hebden Bridge, ISBN 978-0-9534031-0-3, 1998.

Kirkup, S.: The Boundary Element Method in Acoustics: A Survey, Applied Sciences, 9, 1642, https://doi.org/10.3390/app9081642, 2019.

Lacombe, H.: La Houle a La Côte, in: Centre De Recherches et D'etudes Océanographiques, vol. 11, 1950.

Lamb, H.: Hydrodynamics, 6th edn., 1932.

Magne, R., Belibassakis, K. A., Herbers, T. H. C., Ardhuin, F., O'Reilly, W. C., and Rey, V.: Evolution of Surface Gravity Waves over a Submarine Canyon, Journal of Geophysical Research: Oceans, 112, 2005JC003 035, https://doi.org/10.1029/2005JC003035, 2007.

McAllister, M. L., Draycott, S., Calvert, R., Davey, T., Dias, F., and van den Bremer, T. S.: Three-Dimensional Wave Breaking, Nature, 633, 601–607, https://doi.org/10.1038/s41586-024-07886-z, 2024.

Munk, W. and Traylor, M. A.: Refraction of Ocean Waves: A Process Linking Underwater Topography to Beach Erosion, The Journal of Geology, 1947.

Oceanum: Technical Note on Specification and Validation of the Oceanum Global Wave Hindcast, Tech. rep., 2020.

Raichlen, F. and Lee, J.-J.: AN INCLINED-PLATE WAVE GENERATOR, Coastal Engineering, 1978.

Ray, S., De, S., and Mandal, B. N.: Water Wave Propagation over an Infinite Trench, Zeitschrift für angewandte Mathematik und Physik, 73, 46, https://doi.org/10.1007/s00033-022-01682-3, 2022.

Ribal, A. and Young, I. R.: 33 Years of Globally Calibrated Wave Height and Wind Speed Data Based on Altimeter Observations, Scientific Data, 6, 77, https://doi.org/10.1038/s41597-019-0083-9, 2019.

https://doi.org/10.5194/egusphere-2026-2778
Preprint. Discussion started: 1 June 2026

Silva, A. N., Taborda, R., Antunes, C., Catalão, J., and Duarte, J.: Understanding the Coastal Variability at Norte Beach, Portugal, Journal of Coastal Research, 165, 2173–2178, https://doi.org/10.2112/SI65-367.1, 2013.

The WAVEWATCH III R © Development Group (WW3DG): User Manual and System Documentation of WAVEWATCH III ©R Version 6.07, Tech. Note 333, NOAA/NWS/NCEP/MMAB, 2019.

Thomson, J., Elgar, S., and Herbers, T. H. C.: Reflection and Tunneling of Ocean Waves Observed at a Submarine Canyon, Geophysical Research Letters, 32, https://doi.org/10.1029/2005GL022834, 2005.

Thomson, J., Elgar, S., Herbers, T. H. C., Raubenheimer, B., and Guza, R. T.: Refraction and Reflection of Infragravity Waves near Submarine Canyons, Journal of Geophysical Research: Oceans, 112, https://doi.org/10.1029/2007JC004227, 2007.

Tyler, P., Amaro, T., Arzola, R., Cunha, M. R., Stigter, H. D., Gooday, A., Huvenne, V., Ingels, J., Kiriakoulakis, K., Lastras, G., Masson, D., Oliveira, A., Pattenden, A., Vanreusel, A., Weering, T. V., Vitorino, J., Witte, U., and Wolff, G.: Europe's Grand Canyon Nazaré Submarine Canyon, Oceanography, 22, 46–57, 2009.

Vieira, M., Guedes Soares, C., Guimarães, P. V., Bergamasco, F., and Campos, R. M.: Nearshore Space-Time Ocean Wave Observation Using Low-Cost Video Cameras, Coastal Engineering, 197, 104 694, https://doi.org/10.1016/j.coastaleng.2024.104694, 2025.

https://doi.org/10.5194/egusphere-2026-2778
Preprint. Discussion started: 1 June 2026

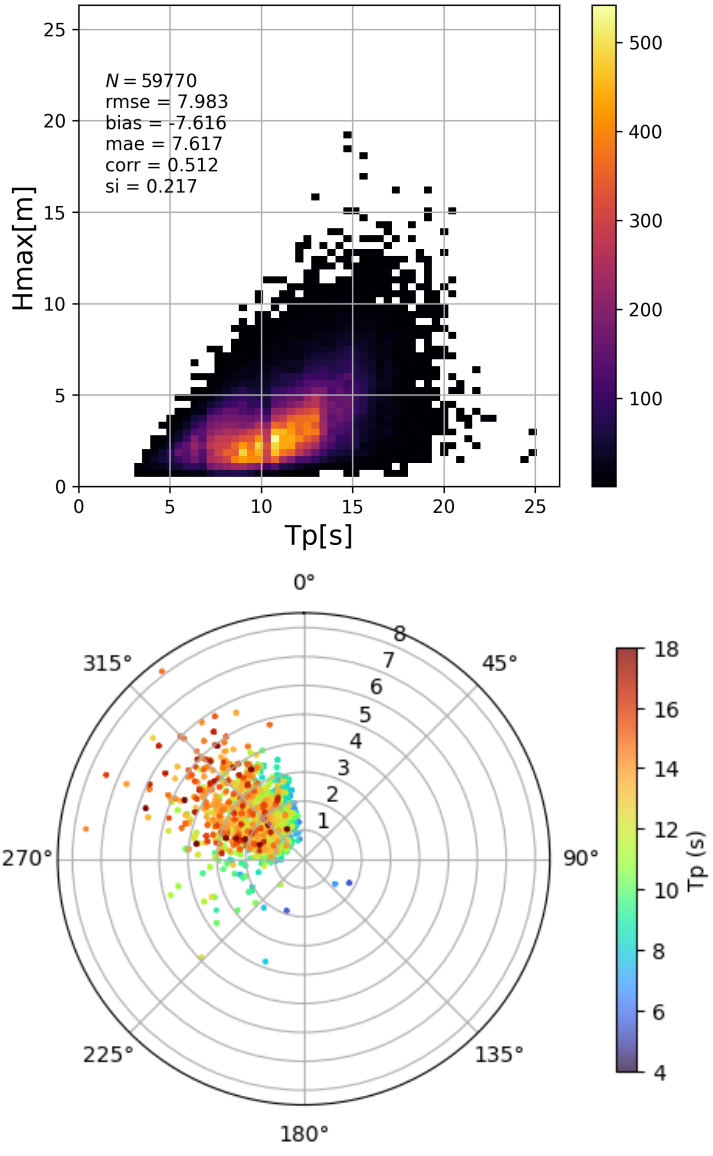

Figure 1. Top: Joint distribution of peak wave period (T_p) and maximum wave height ($H_{\max}$) measured by an offshore wave buoy maintained by Hydrographic Institute of the Portuguese Navy, in Nazaré (Portugal) over the period 2009–2025. Colors indicate the frequency of occurrence (number of observations per bin). Statistical metrics are reported in the panel based on a total of $N = 72,311$ observations. **Bottom:** Peak wave period (T_p) distribution as a function of wave direction derived from WW3 hindcast validated with altimeter data over the period 1992–2024 (Oceanum, 2020; Ribal and Young, 2019). Radial axis shows H_s, points are colored by T_p (in seconds). The plot highlights the dominant directional sectors and their associated wave periods over the observed period.

https://doi.org/10.5194/egusphere-2026-2778
Preprint. Discussion started: 1 June 2026

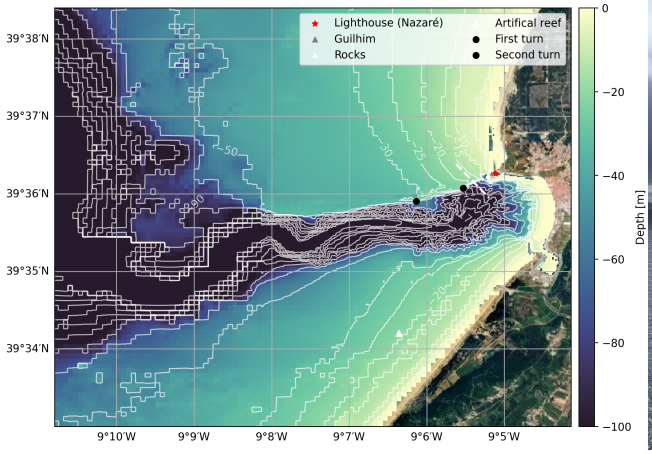

(a) *Bathymetry outside Nazaré:* The canyon terminates south of the lighthouse. North of the lighthouse is the Praia do Norte beach where the most intense focusing occurs. (Bathymetry: EMODnet Bathymetry Consortium (2022). Map data and Imagery © 2024 Google, Data SIO, NOAA, U.S Navy, NGA, GEBCO, Airbus, Maxar Technologies).

(b) A view westwards from the fort, where the stereo-cameras were located for the first setup. The rocks are roughly aligned with the northern canyon edge.

(c) Photo taken the year before, November 2023, from the lighthouse towards the north-west showing how the interference of reflected and incident waves form pyramid-shaped waves.

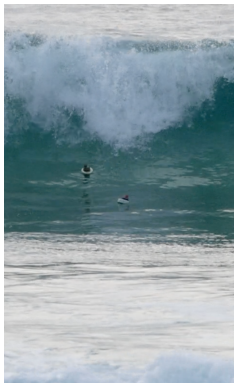

(d) The SFY-buoys were deployed in a cross pattern extending from the rocks and outwards, before they drifted into the breakers on the North-beach.

(e) The stereo-cameras looking Northwards along the beach for the second setup (photo taken the year before, November 2023).

Figure 2. Overview of the canyon, measurement methods (stereo-cameras and wave buoys), and experiment areas.

https://doi.org/10.5194/egusphere-2026-2778
Preprint. Discussion started: 1 June 2026

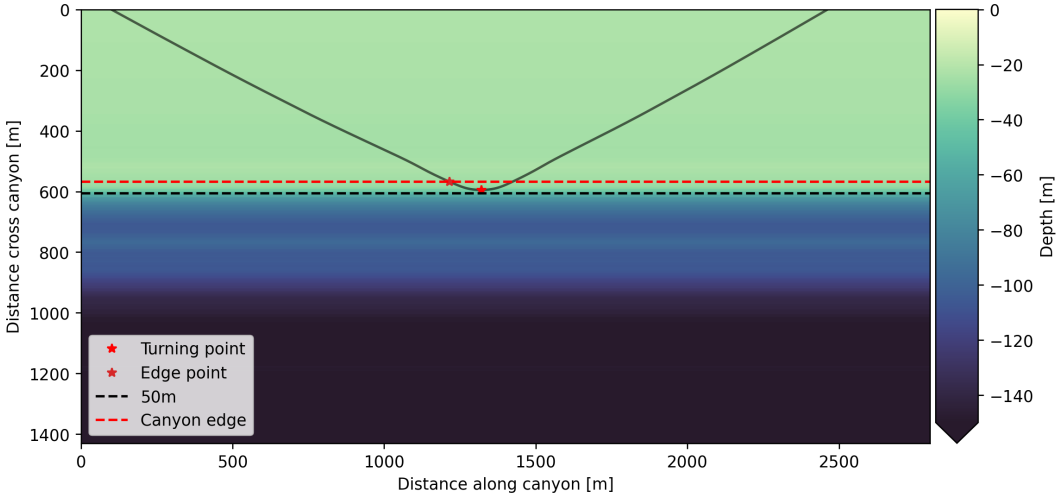

(a) Refracted ray at the canyon edge of an idealized 1D depth-profile of the shelf and canyon edge.

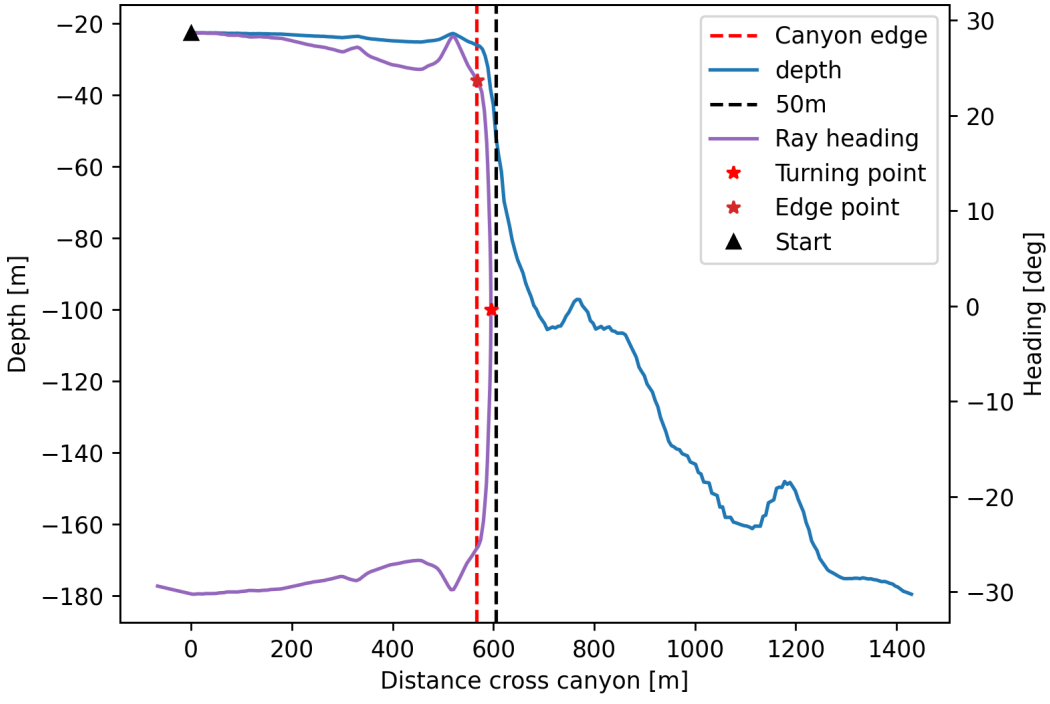

(b) Change of ray direction as it approaches the canyon edge.

Figure 3. Refraction of wave rays because the shelf slopes slightly towards the canyon, causing the incident angle at the canyon edge to *increase* before being reflected (or strongly refracted) by the depth change at the canyon cliff.

https://doi.org/10.5194/egusphere-2026-2778
Preprint. Discussion started: 1 June 2026

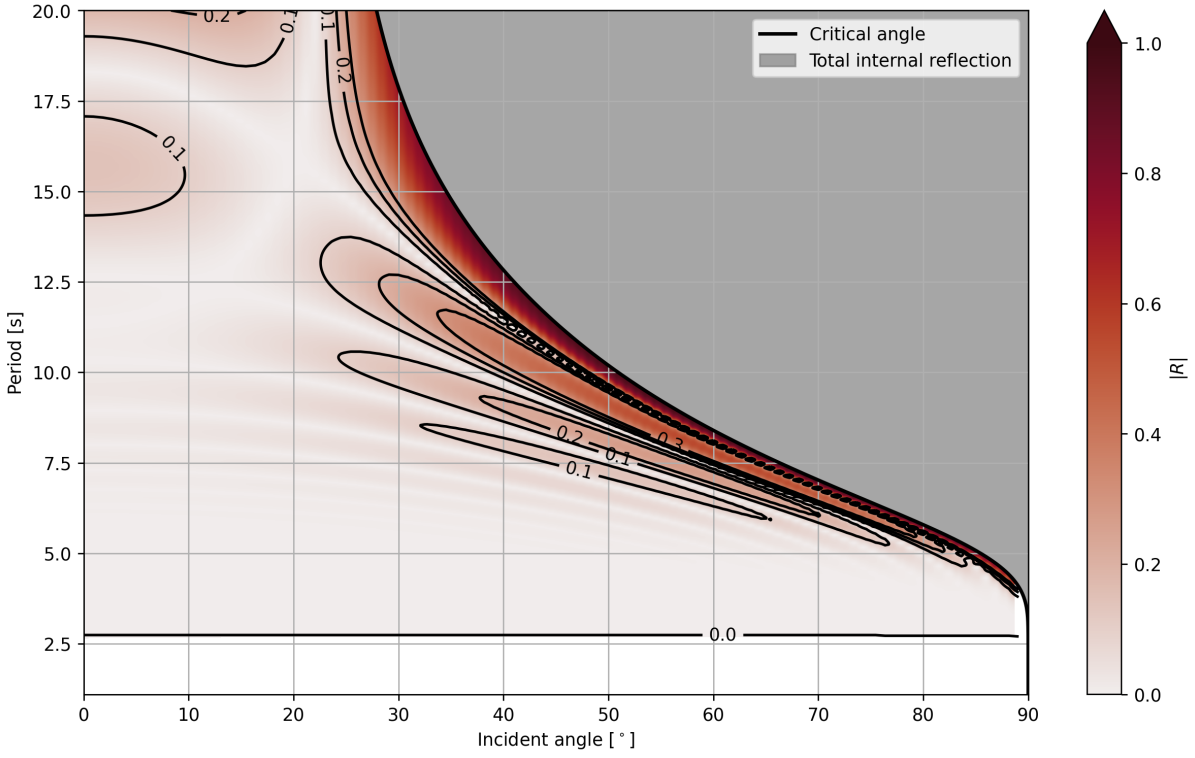

(a) Reflection coefficient ($|R|$). The contour of the critical angle where the cross-canyon wavenumber is imaginary, and the wave encounters total internal reflection. $h_1 = 20$ m, $h_2 = 150$ m, $h_3 = h_1$, $L = 250$ m.

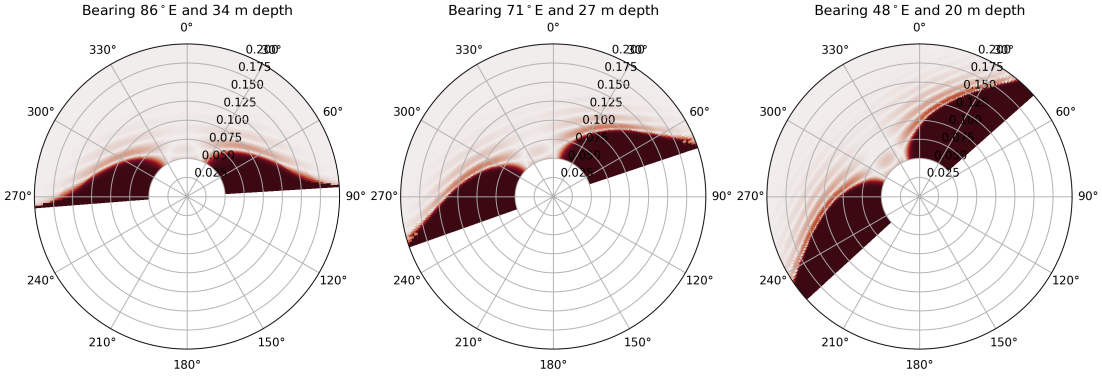

(b) The reflection coefficient (with incidence angle modified by refraction, Fig. 3) as a function of wave direction (coming from), wave period (frequency), and onto different canyon edge segments with different orientations. The shelf depth is 34, 27, and 20 meters from the left, shallower shelf depth cause greater reflection.

Figure 4. Reflection coefficient using the plane-wave approximation (*PWA* from Kirby and Dalrymple (1983), Eq. 4.4).

https://doi.org/10.5194/egusphere-2026-2778
Preprint. Discussion started: 1 June 2026

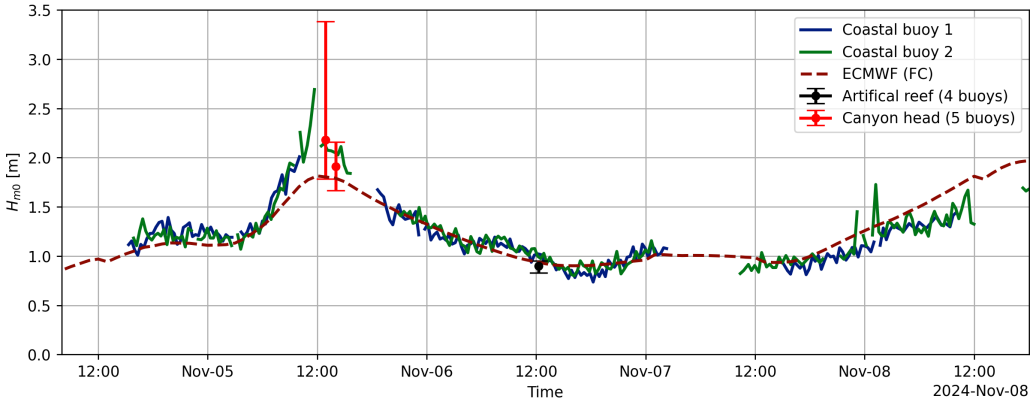

(a) H_{m0} throughout the experiment. Measured by free-drifting buoys drifting northward along the coast.

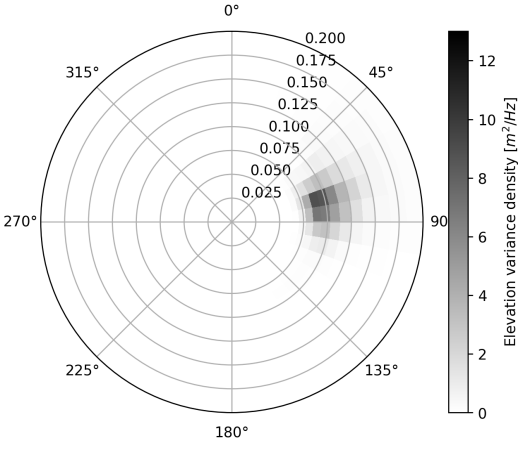

(b) ECMWF directional spectrum forecasted for Tuesday 5th November 2024 at 13:00 (direction going towards).

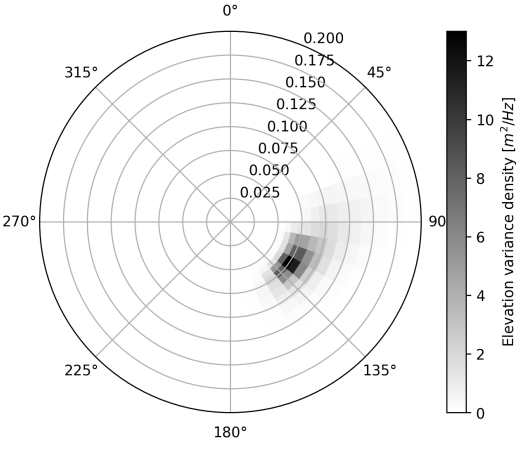

(c) ECMWF directional spectrum forecasted for Friday 8th November 2024 at 16:00 (direction going towards). This spectrum is typical for Nazaré (Fig. 1).

Figure 5. Wave conditions throughout the experiments in November 2024.

https://doi.org/10.5194/egusphere-2026-2778
Preprint. Discussion started: 1 June 2026

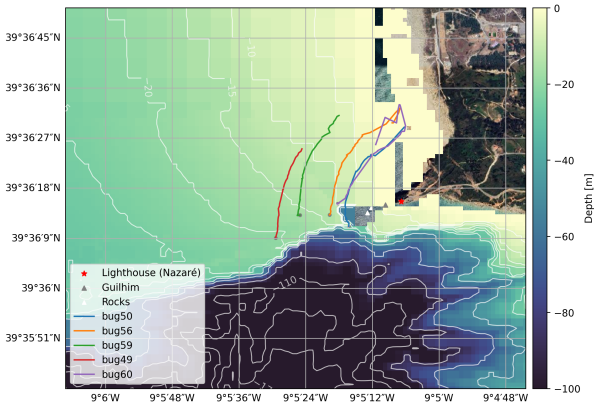

(a) *Experiment #1: Tue. 5th November 2024 at 12:51*: Buoy trajectories. Buoy *49* is located furthest towards sea.

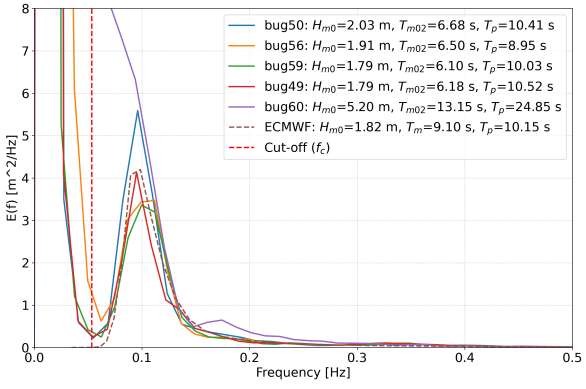

(b) Elevation energy spectrum of waves measured by buoys and forecast by ECMWF. The buoy located furthest towards sea have a spectrum closest to the one predicted by ECMWF. All the buoys are located **on the shelf**.

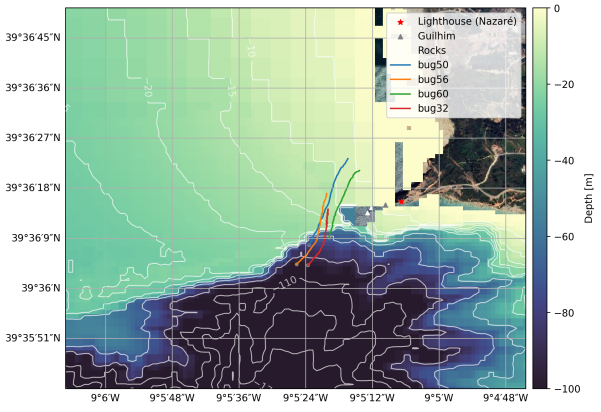

(c) *Experiment #2: Tue. 5th November 2024 at 14:03*: Buoy trajectories. Buoy *56* is located furthest towards sea.

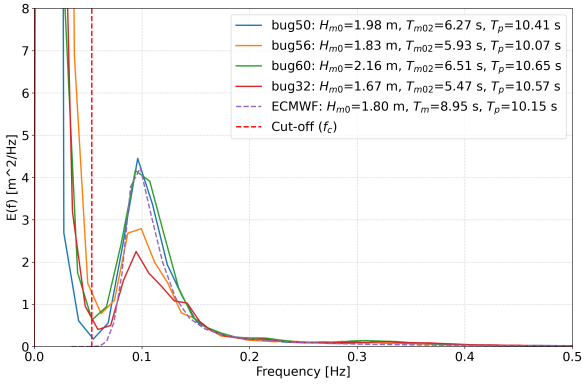

(d) Elevation energy spectrum of waves measured by buoys and forecast by ECMWF. The buoys located **on the shelf** have a spectrum closest to the one predicted by ECMWF.

Figure 6. Experiments 1 and 2: High-pass cut-off frequency for calculated H_{m0} for the buoys is shown in red. Forecasted mean (MWD) and peak wave direction (PWD) is 72 and 70 degrees or from west-southwest.

https://doi.org/10.5194/egusphere-2026-2778
Preprint. Discussion started: 1 June 2026

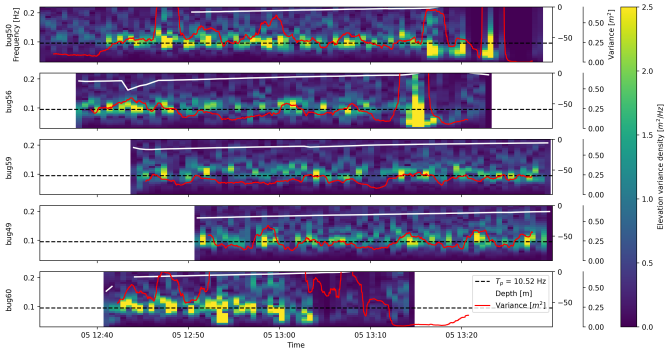

(a) Spectrogram recorded by buoys in refraction experiment #1.

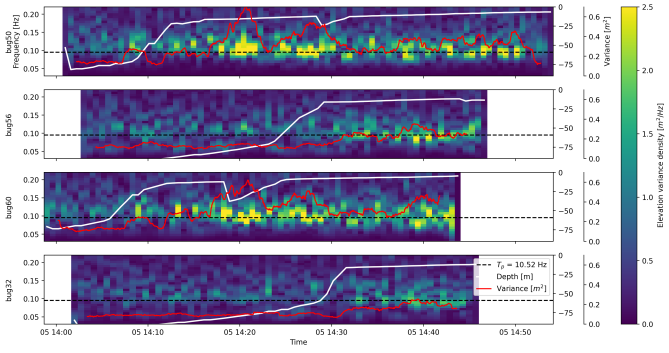

(b) Spectrogram recorded by buoys in refraction experiment #2.

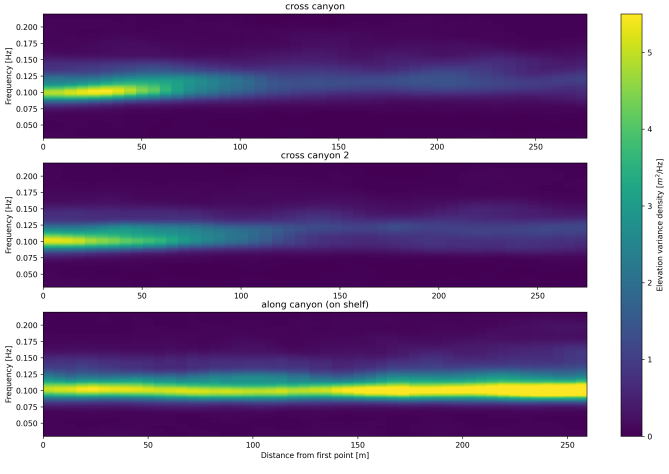

(c) Spectrograms (10 minute window) recorded for sample transects by stereo-video cameras. The position of the transects are shown in Figure 9c.

Figure 7. Spectrogram from refraction experiment 1 and 2.

https://doi.org/10.5194/egusphere-2026-2778
Preprint. Discussion started: 1 June 2026

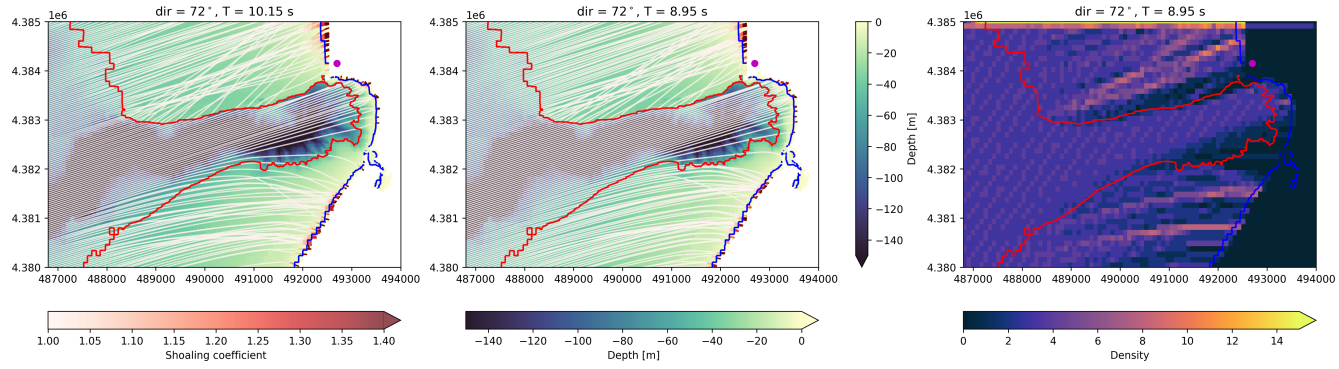

(a) Overview of rays.

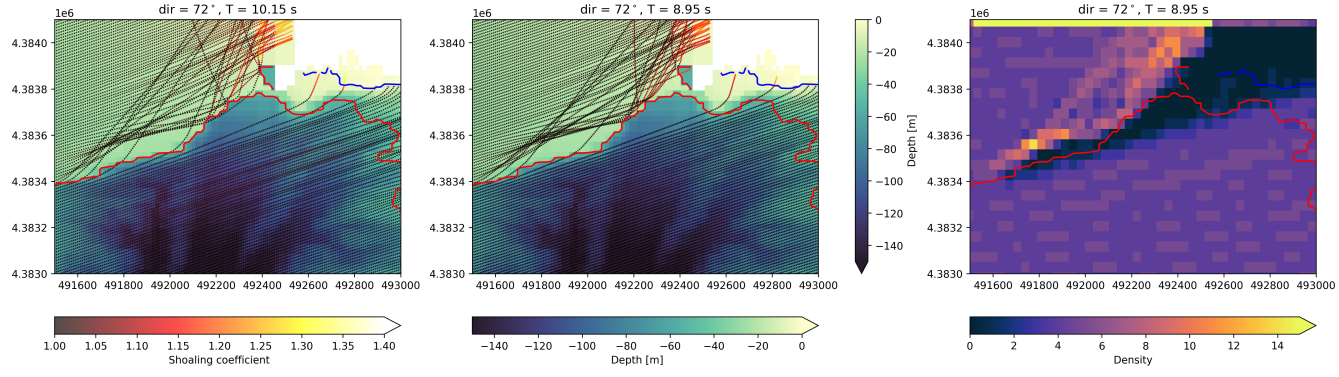

(b) Rays above the canyon terminus.

Figure 8. Rays traced for experiment #1 and #2: $T_p = 10.15$ s, and $T = 8.95$ s with direction towards 72°. The position of the lighthouse is shown as a dot.

https://doi.org/10.5194/egusphere-2026-2778
Preprint. Discussion started: 1 June 2026

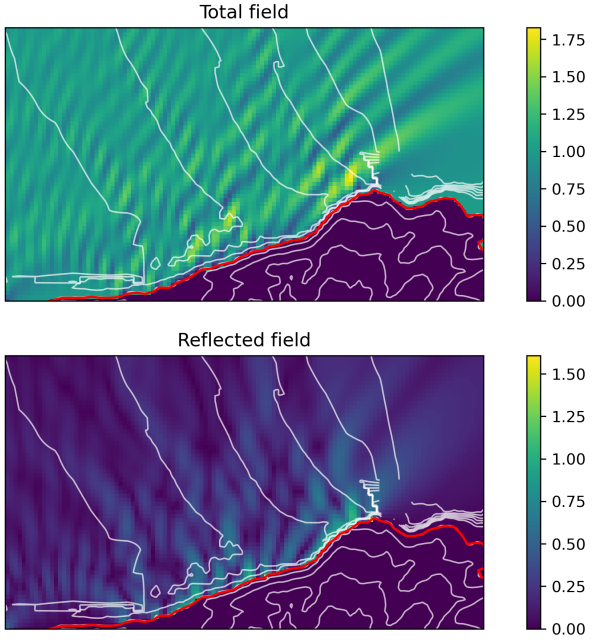

(a) Amplitude response of coherent superposition of incident and reflected wave field of the peak wave component.

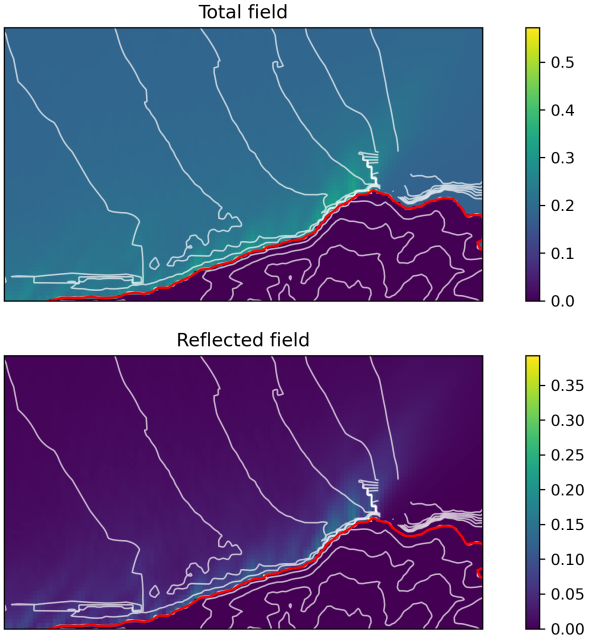

(b) Variance (m_0) of wave field for forecasted ECMWF directional spectrum. The components are incoherently summed (Eq. (3)).

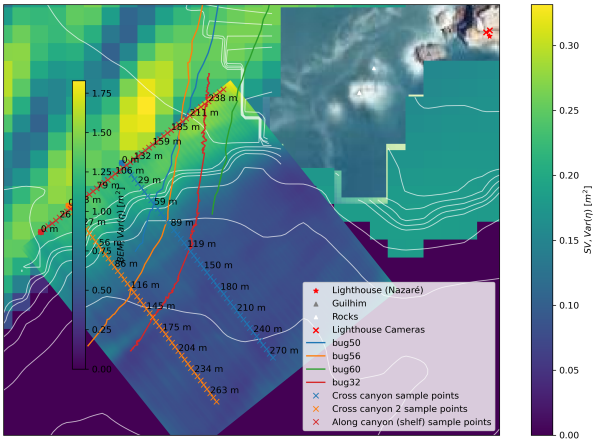

(c) BEM (total field) of peak period (Fig. 9a), with *measured* stereo-video variance overlaid.

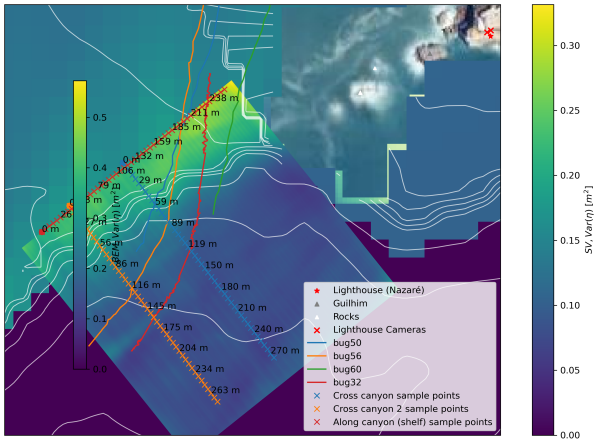

(d) Variance (m_0) of BEM modeled total-field with incoming full ECMWF spectrum (Fig. 9b). Stereo-video variance is overlaid.

Figure 9. *Along-canyon waves.* **Top:** Amplitude and sea-surface variance (m_0) calculated using BEM for forecasted ECMWF directional spectrum (Fig. 5b), white contours show water depth. **Bottom:** Stereo-video sea-surface variance compared with BEM model. Buoy tracks for spectrograms shown in Fig. 6d are also plotted. Cross-lines show the sample transects for the stereo-video spectrograms (Fig. 7c).

https://doi.org/10.5194/egusphere-2026-2778
Preprint. Discussion started: 1 June 2026

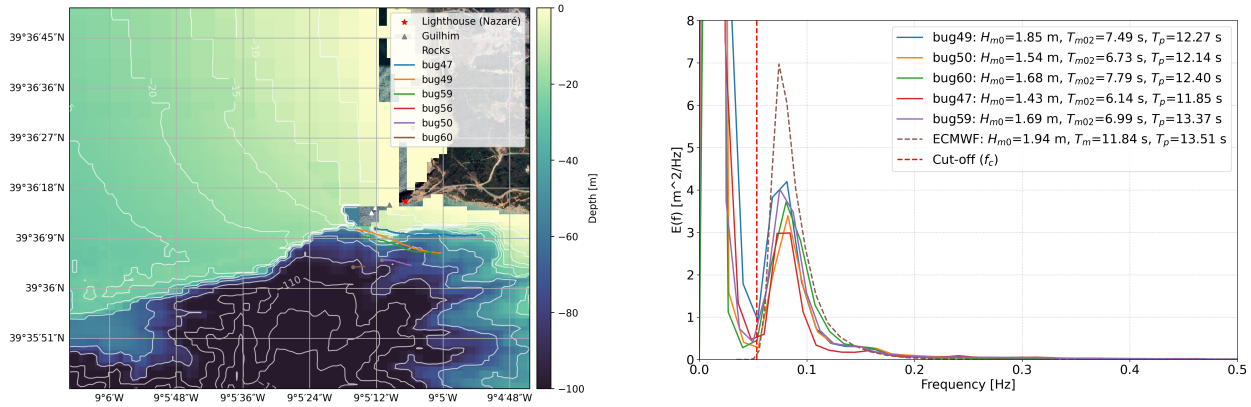

(a) *Experiment #3: Fri. 8th November 2024 at 15:40*: Buoy trajectories. Buoy *60* is located furthest towards sea.

(b) Elevation energy spectrum of waves measured by buoys and forecast by ECMWF.

Figure 10. Buoy drift paths, measured and forecasted spectra. All the buoys are **above the valley**, and show a significantly lower amplitude around the peak period compared to the forecasted spectrum. High-pass cut-off frequency for the calculated H_{m0} for the buoys is shown in red. Forecasted MWD and PWD is 111 and 120 degrees, or from north-northwest.

https://doi.org/10.5194/egusphere-2026-2778
Preprint. Discussion started: 1 June 2026

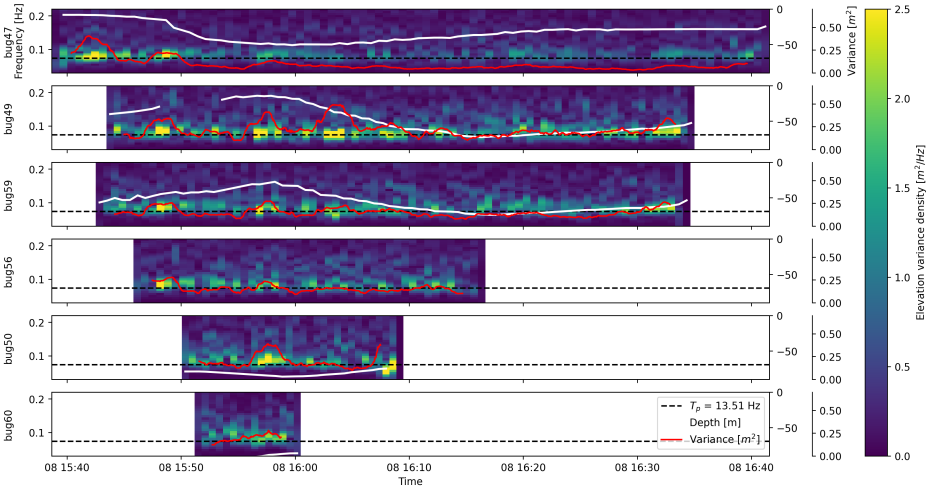

(a) Spectrograms measured by the buoys on Friday 8th of November 2024. The depth below the buoys is shown in white. The rolling-window variance is shown in red.

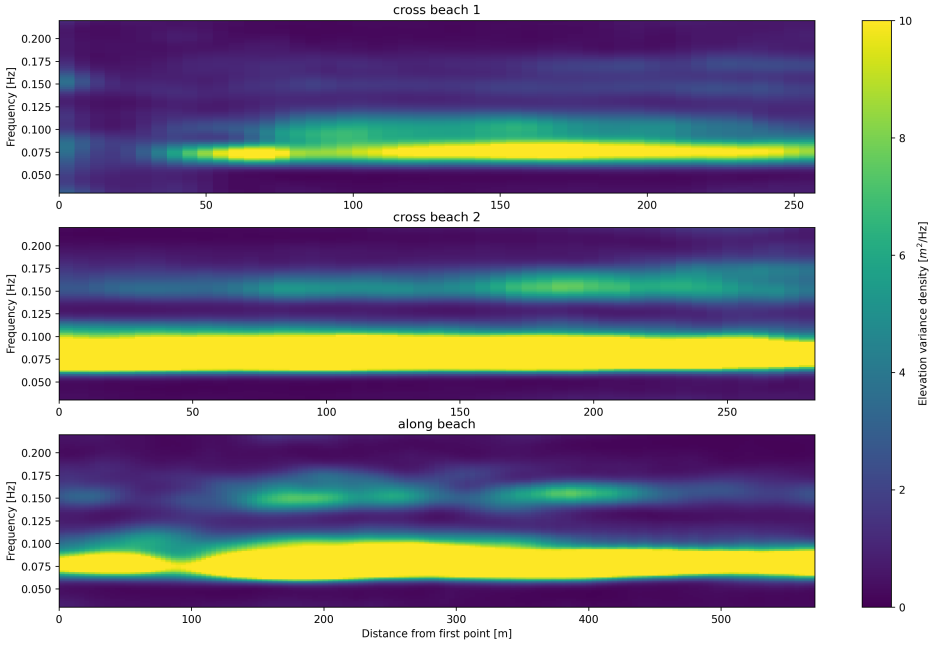

(b) Spectrograms for virtual sample points in Fig. 13c.

Figure 11. Reconstructed sea-surface and variance along marked lines, measured by stereo-video cameras on Friday 8th of November, 2024. The stereo-cameras are pointed towards the north-north-west so along the beach.

https://doi.org/10.5194/egusphere-2026-2778
Preprint. Discussion started: 1 June 2026

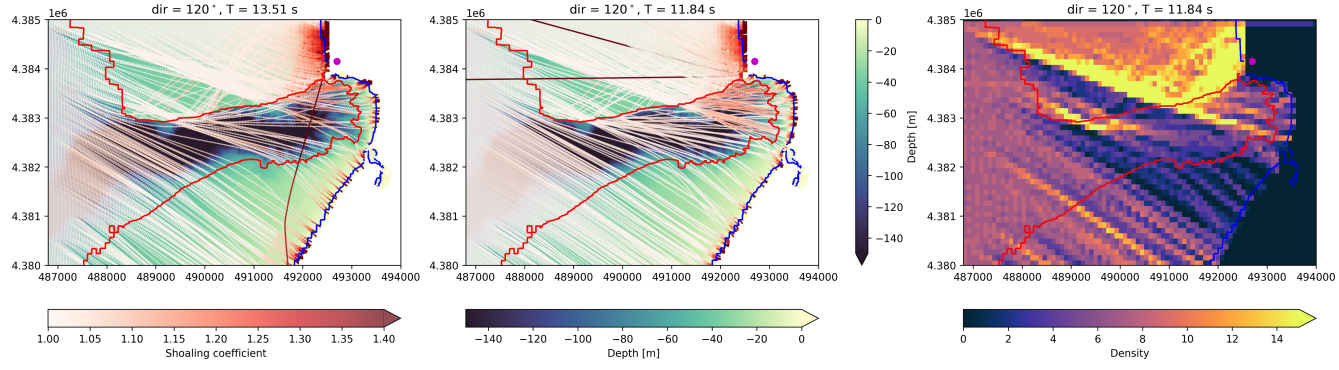

(a) Overview of rays.

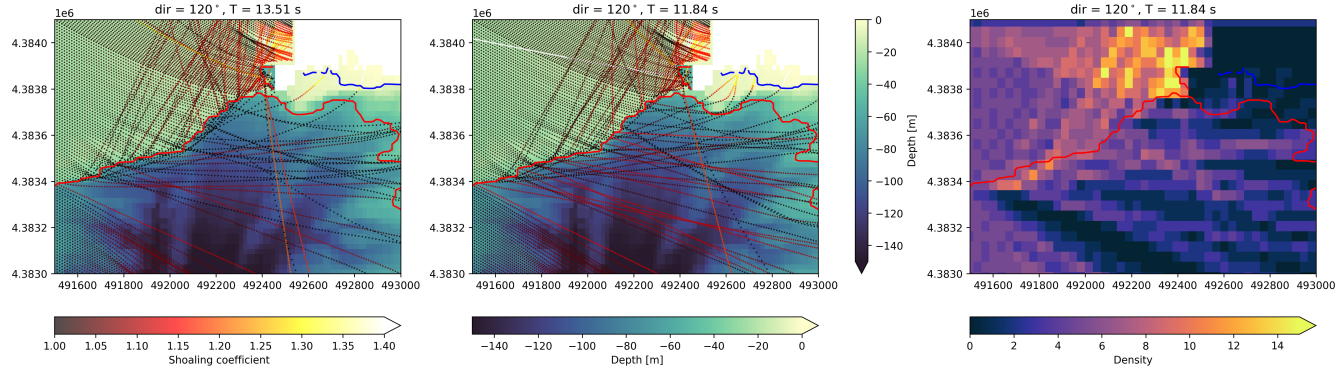

(b) Rays above canyon terminus.

Figure 12. Rays traced for experiment #3: $T_1 = 13.51$ s, $T_2 = 11.84$ s and direction towards 120°. The position of the lighthouse is shown as a dot.

https://doi.org/10.5194/egusphere-2026-2778
Preprint. Discussion started: 1 June 2026

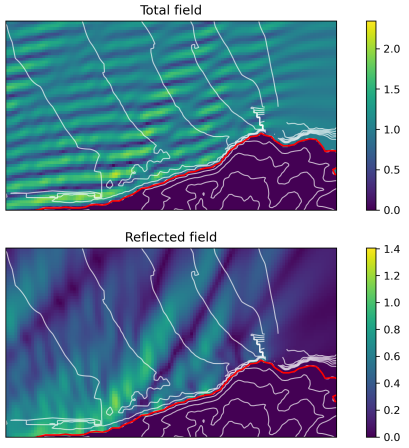

(a) Amplitude response of coherent superposition of incident and reflected wave field of the peak wave component.

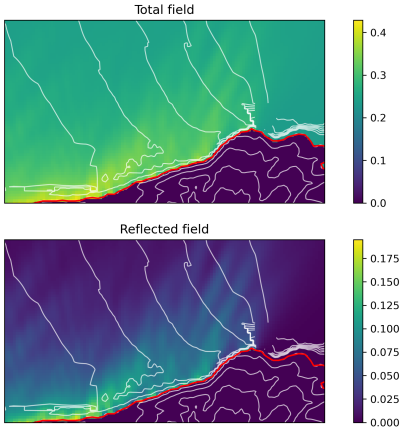

(b) Variance (m_0) of wave field for forecasted ECMWF directional spectrum. The components are incoherently summed ((3)).

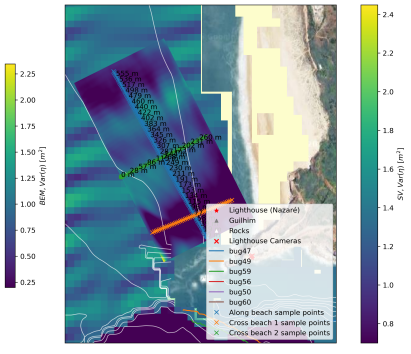

(c) BEM-modeled incident and reflected field (amplitude) of peak period with measured variance from stereo-cameras overlaid.

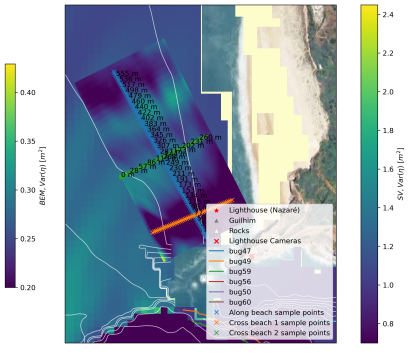

(d) BEM-modeled variance (m_0) using ECMWF spectrum with measured variance overlaid.

(e) Photo from the lighthouse towards the north at 15:57 (UTC). Peaks are formed along the beams.

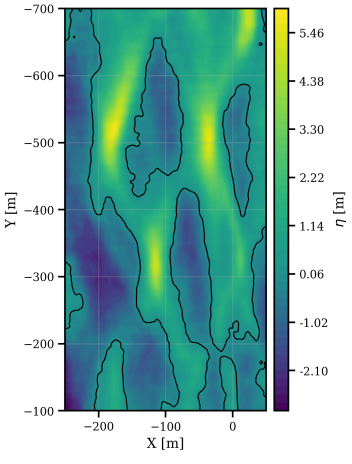

(f) Stereo-camera re-constructed surface towards the north at 16:10 (UTC).

Figure 13. *Oblique waves.* Amplitude and sea-surface variance (m_0) calculated using BEM for forecasted ECMWF directional spectrum (Fig. 5c), and overlaid with measured variance from stereo-cameras. The BEM-model does not take into account the change in incidence angle due to refraction before the canyon edge. The waves were breaking with a face-height of up to 7 meters.

https://doi.org/10.5194/egusphere-2026-2778
Preprint. Discussion started: 1 June 2026

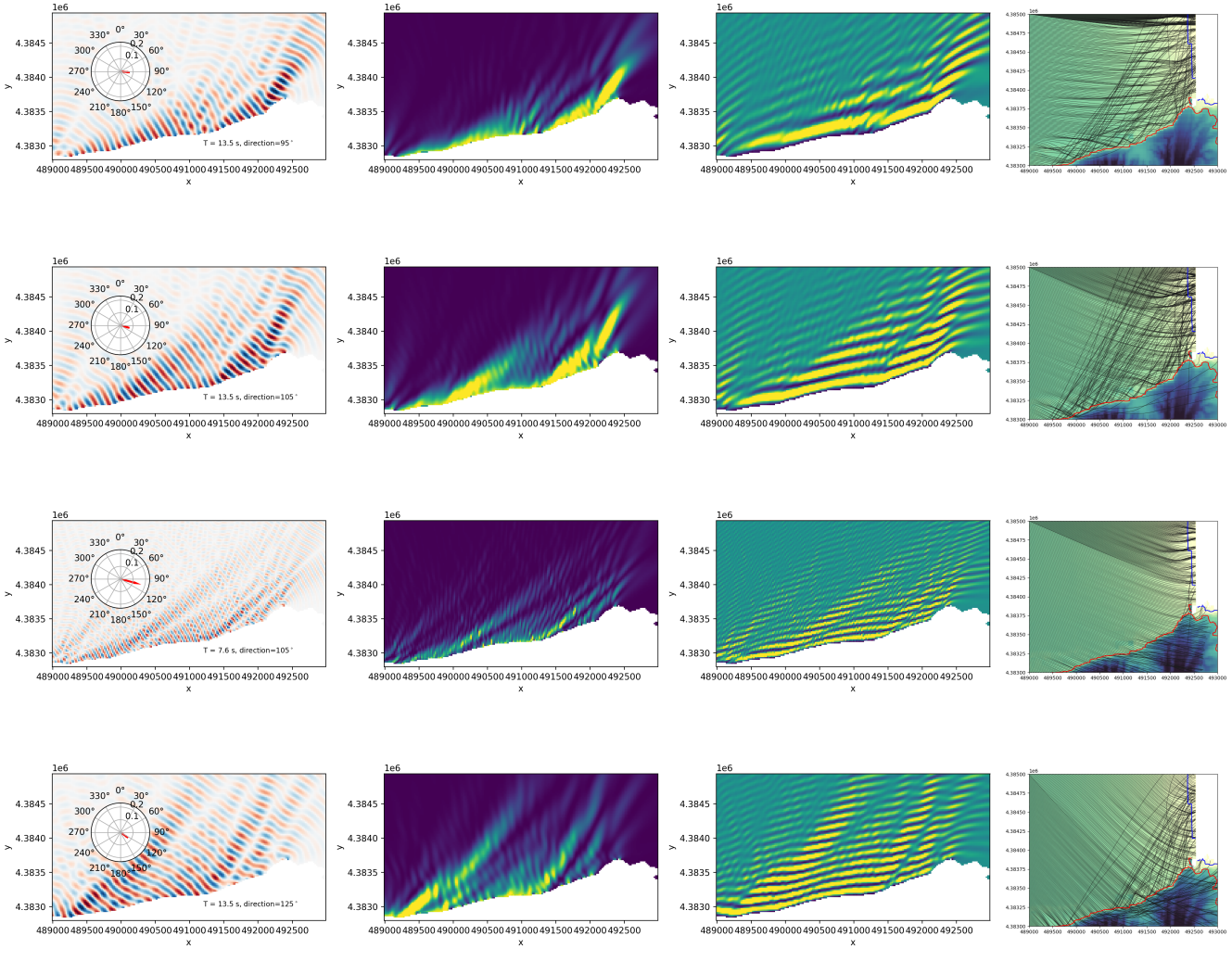

Figure 14. BEM and ray-tracing simulations of the wave fields with incoming waves heading towards 95°, 105°, 105°, and 125° with period 13.5 s, 13.5 s, 7.6 s, 13.5 s, respectively. From the left in each panel: the reflected field amplitude (BEM), reflected field variance (m_0, BEM), total field variance (m_0, reflected and incident field coherently summed, BEM), and incident rays refracted. Waves traveling towards directions between 95° and 125°, with periods greater than about 7 seconds, cause significant focusing. Inset spectrum in left-most panel show the frequency and direction.

https://doi.org/10.5194/egusphere-2026-2778
Preprint. Discussion started: 1 June 2026

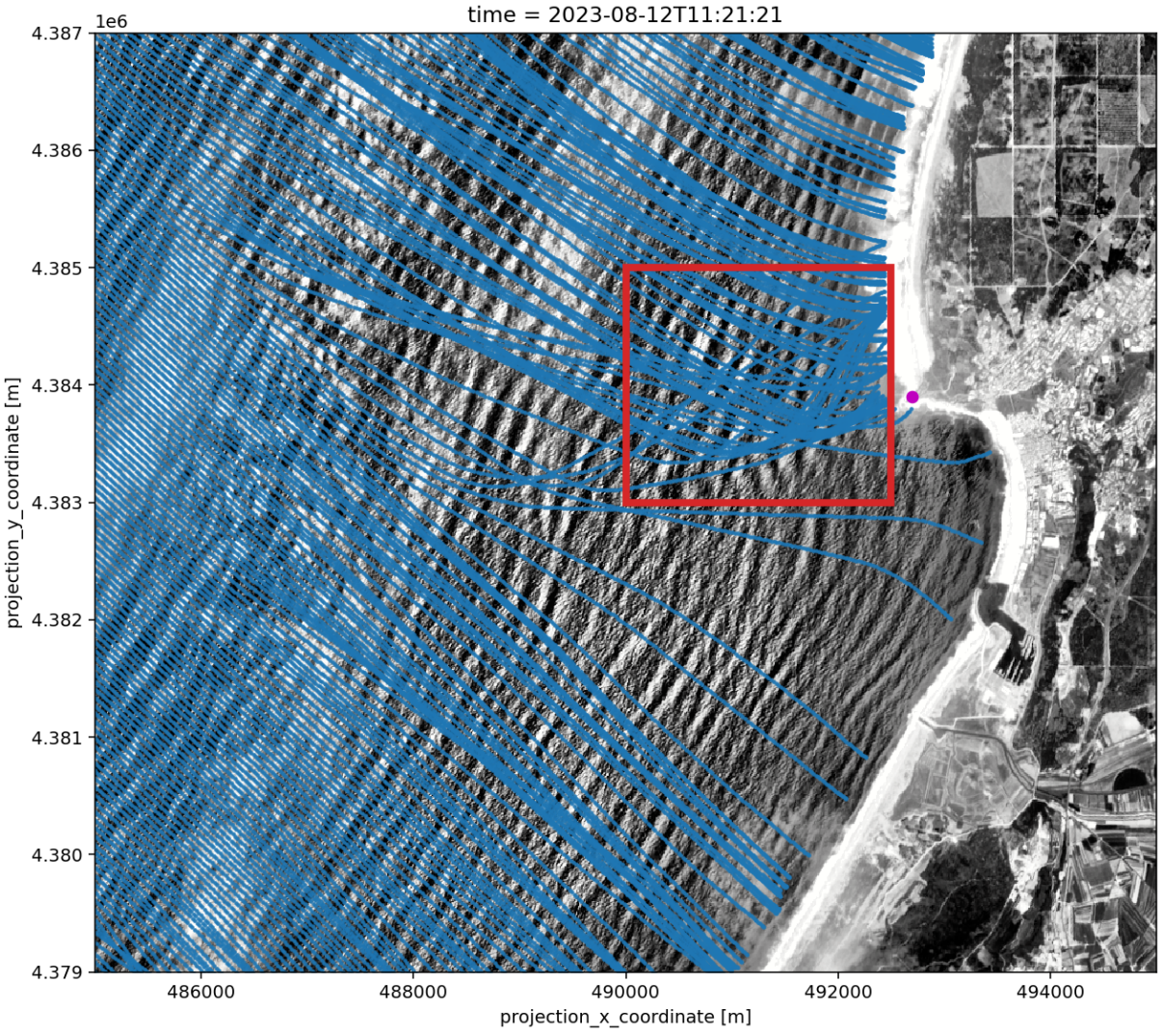

Figure 15. Rays on top of a satellite image from the previous year (2023-08-12T11:21:21) with waves of approximately 12.1 s period arriving from the North-West. Image contains modified Copernicus Sentinel-2 Level-1C data (2023).